JOURNAL OF MATERIALS SCIENCE 11 (1976) 1393–1418

The rheology of a partially solid alloy

P. A. JOLY*
Massachusetts Institute of Technology, Cambridge, Massachusetts, USA

R. MEHRABIAN
Department of Metallurgy and Mining Engineering, and the Department of Mechanical and Industrial Engineering, University of Illinois, Urbana, Illinois, USA

The effect of various thermomechanical treatments on the structure and rheological behaviour of Sn–15% Pb alloy in its solidifcation range was investigated using a concentric cylinder viscometer. The apparatus was designed to permit wide ranges of cooling rates up to 25° C min^{-1} and shear rates up to 750 sec^{-1}. Initially, the alloy was continuously sheared as it cooled from above the liquidus to a desired volume fraction solid. In one series of experiments, shear was stopped and the alloy quenched. In a second series, the alloy was held isothermally and subjected to various mechanical treatments. The size and morphology of primary solid particles during continuous cooling is influenced by shear and cooling rates and volume fraction of solid – faster cooling results in finer structures while increased rate of shear reduces the amount of entrapped liquid in individual particles. The viscosity of the slurry, at a given volume fraction solid, decreases with decreasing cooling rate and increasing shear rate. Exercising the full range of shear and cooling rates possible in the viscometer, the apparent viscosity of a 0.55 volume fraction solid slurry varied from 3 to 80 P. The structure and viscosity of isothermally held slurries follow the same trends as slowly cooled slurries. However, their viscosity at a given volume fraction solid is consistently lower than that of continuously cooled slurries. The slurries are thixotropic and show a hysteresis loop phenomenon similar to other well known thixotropic systems. Measured areas of hysteresis loops increase with increasing volume fraction solid, initial viscosity and time at rest. The potential applications to improve existing or develop new metal-forming processes are being investigated in a variety of alloys with different solidifcation ranges and temperatures.

1. Introduction

Until recently, almost all commercial metal-forming processes were carried out either in the fully solid or fully liquid condition. This is because, solidification in usual castings and ingots is dendritic. The growing dendrites form a continuous skeleton in the liquid–solid zone when the volume fraction of solid exceeds approximately 0.2. Thereafter, the alloy can neither be poured successfully to allow solidification processing, nor can it be deformed homogeneously, without cracking to allow deformation processing.

Recent work has shown that vigorous agitation of a metal alloy postpones the formation of a continuous solid network to much higher fractions solid [1]. The primary solid forming is non-dendritic and spheroidal in shape. The resulting partially solidified metal slurry has a measurable low viscosity, deforms homogeneously, hence it lends itself to various new forming processes. Fig. 1 shows the structures of a normally solidified and a vigorously agitated Sn–15% Pb alloy deformed in the annular space of a high temperature viscometer [1]. In Fig. 1a a typical dendritic microstructure of the alloy in the partially solid state was subjected to a moderate amount of strain. Grains are seen to have been pulled apart and some bending and fracture of

* Present address: Corning Research Inc, Avon, France.

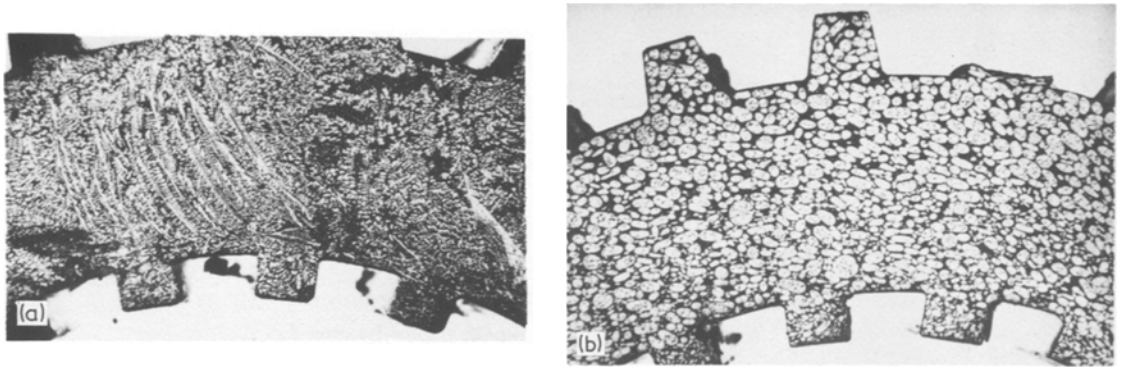

Figure 1 Structures of Sn–15% Pb alloy subjected to different thermomechanical treatments in the solidifcation range at × 5.5. (a) The sample was cooled to 0.36 volume fraction solid and subjected to shear. (b) The sample was sheared and cooled continuously to 0.60 volume fraction solid and quenched [1].

dendrites is also apparent. The structure of the alloy subjected to vigorous agitation during solidification is shown in Fig. 1b. The relative ease with which shear can take place in this continuously sheared specimen results from the fact that the solid is present as a suspension of small rounded grains. In this sample, deformation was homogeneous across the annular gap.

A further experimental observation was that the apparent viscosity of metal slurries, prepared in this way, decreases with increasing rate of shear [1]. The slurries were described as being thixotropic. However, no specific method was used to measure and characterize this rheological behaviour. In this study the technique developed by Green and Weltmann [2] was used to characterize thixotropy. It consists of measuring a hysteresis loop. They used a rotational viscometer in which the angular velocity could be varied continuously. The procedure commences

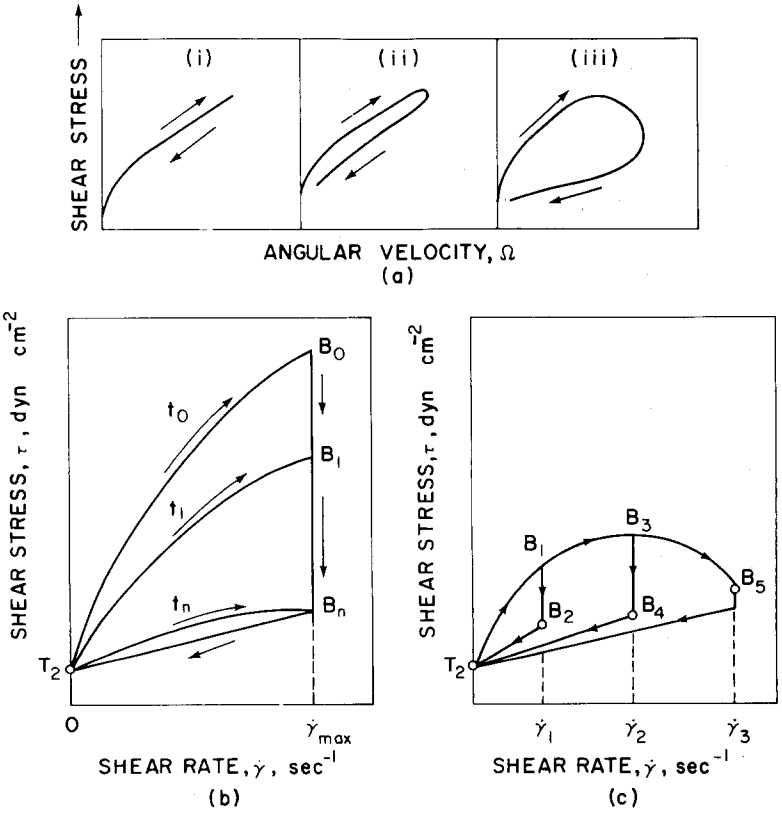

Figure 2 Hysteresis loops of (a) three different materials showing (i) no, (ii) little, and (iii) high thixotropy, respectively; (b) thixotropic material when the up-time is increased; (c) when the maximum shear rate is increased [2].

with an up-curve, starting at zero speed. The speed is then increased continuously while measuring the change in induced torque. At some specified upper rotational limit, the speed is either maintained constant and then reversed or simply reversed to zero and a down-curve is measured. If the material is thixotropic, the up- and down-curves (i.e. torque versus shear rate) when plotted together will not coincide, thus forming a loop. This condition is ascribed to a structural breakdown. A large loop means considerable breakdown while a small loop signifies small breakdown, or little thixotropy (Fig. 2a). This quantitative description of thixotropy (i.e. area of the hysteresis loop) is also affected by the time it takes to attain the desired maximum shear rate itself.

Fig. 2b shows how the time it takes on the up-curve to reach the maximum shear rate, $\dot{\gamma}_{max}$, affects the corresponding maximum torque value. For short times, $t = t_0$, the path followed is denoted as T_2B_0. With increasing times, the torque necessary to sustain a given shear rate decreases (e.g., for $t = t_1$), the path followed is T_2B_1. After reaching the maximum shear rate the corresponding torque decreases to a steady state value with time, at B_n(Fig. 2b). The down-curve, B_nT_2, is then obtained by decreasing shear rate back to zero.

If the rate of increase of the shear rate is kept constant, while the magnitude of the maximum shear rate is increased, the area of the loop increases. For example, thixotropic material sheared along the path T_2B_1 reaches a maximum shear rate of $\dot{\gamma}_1$, and has a corresponding hysteresis loop area enclosed by $T_2B_1B_2T_2$, (Fig. 2b).

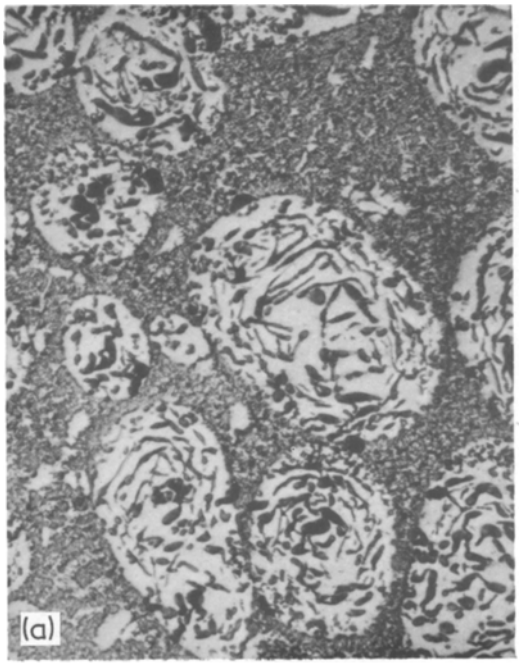

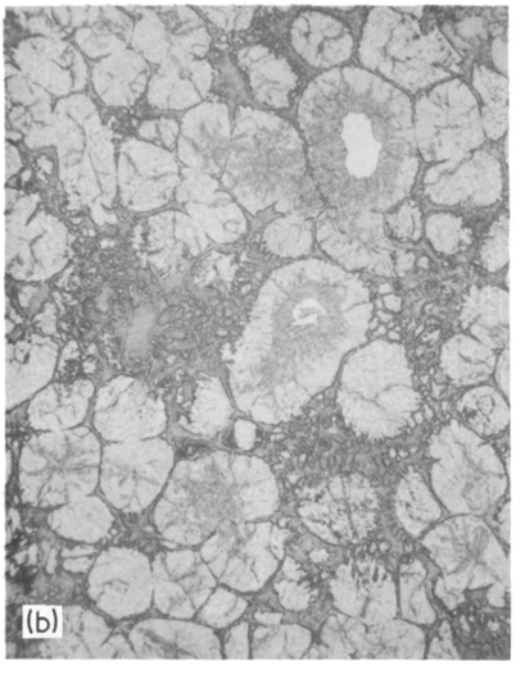

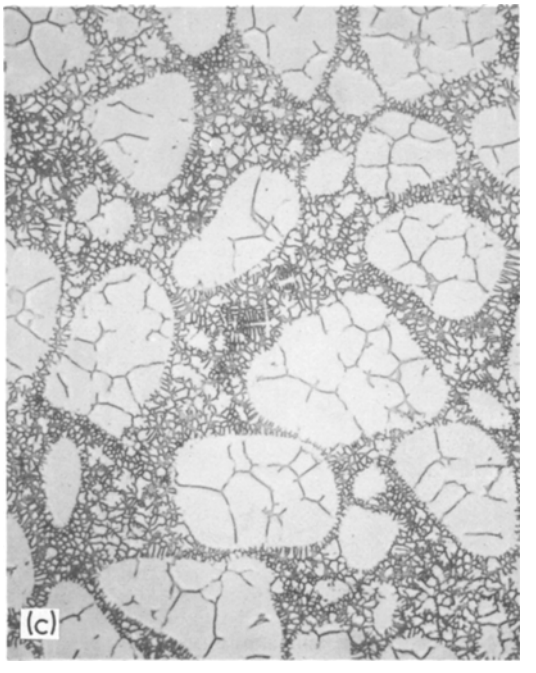

Figure 3 Microstructures of alloys obtained by water-quenching partially solidified, vigorously agitated, samples × 100; (a) Fe–3% C–4% Si cast iron, (b) 440 stainless steel, (c) cobalt-base alloy H.S. 31 [5].

With increasing maximum shear rates, $\dot{\gamma}_2$ and $\dot{\gamma}_3$, the area enclosed by the hysteresis loop increases.

Both the special structure and the associated rheological properties of vigorously agitated slurries have been observed in a variety of alloys with different melting points and solidification temperature ranges. These include aluminium, bronze, cast iron, stainless steel and superalloys. Fig. 3 shows representative microstructures of a cast iron, a stainless steel, and a cobalt base superalloy. These were obtained by direct water quenching of the partially solidifed slurries. The fine dendritic matrix structures resulted from the rapid solidifcation of that portion of the alloys which was liquid prior to the quench.

In the last three years extensive engineering work has been carried out to develop new, or improve existing metal-forming processes based on the above findings. One such process, work on which is presently underway, is machine casting of high temperature alloys employing semi-solid metals as charge material [3–5]. Another potential application is in making metal-particulate or fibrous non-metal composites. The non-metals can be readily introduced and retained into the partially solid metal slurries [5].

In order to successfully apply this new technology, a better understanding of the rheological behaviour of partially solidifed, vigorously agitated metal slurries is necessary. It is to this end that the present fundamental study was undertaken. The two goals of the work were to relate the structure of a metal alloy slurry to process variables, and to determine the relationship between rheological behaviour and structure.

2. Apparatus and procedure

2.1. Viscometer

The high temperature Couette viscometer with accurate independent temperature control previously developed [1] was used in this study (Figs. 1 and 4). The metal alloy resides in an annular space between an outer cylinder (cup)

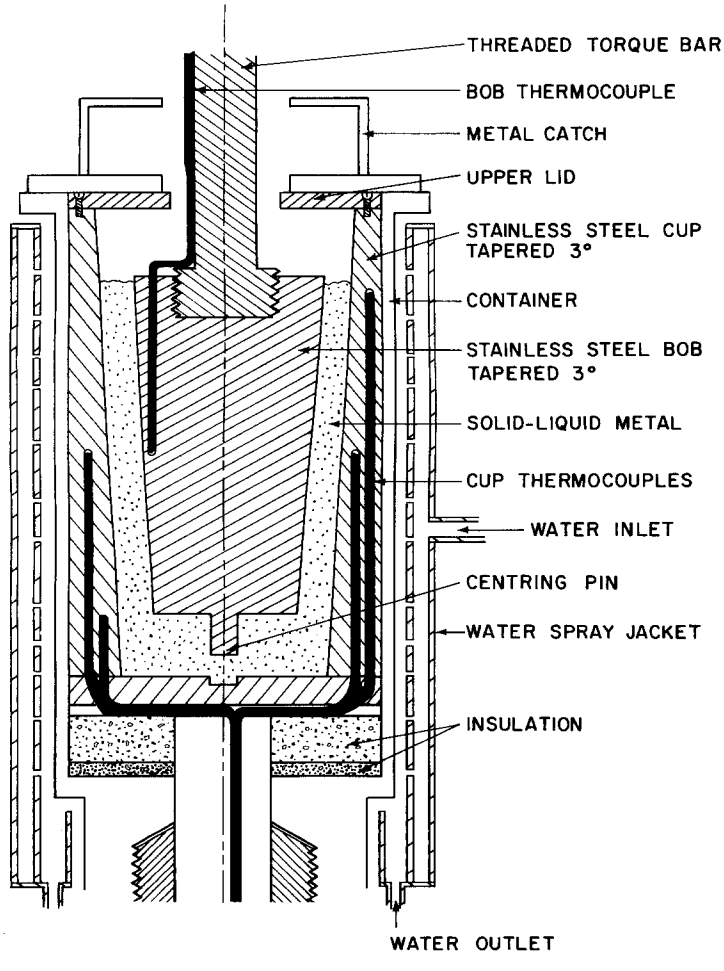

Figure 4 Schematative diagram of apparatus.

and an inner cylinder (bob). The cup is rotated while torsional forces on the stationary bob are measured with a torque dynamometer composed of a flexture pivot with a microsyn and rotor. The flexture pivot converts torque to an angular deflection and the microsyn and rotor transposes this angular deflection into a calibrated voltage output. Apparent viscosity is then calculated as described in Appendix 1.

Two different cup and bob arrangements were used with corresponding annular gaps of 3 and 9 mm. Exact dimensions are given in Appendix 1. Both cup and bob were machined from 304 stainless steel. Vertical grooves (ribs) 4 mm wide by ~1 mm deep were machined along the faces of the cup and bob to prevent slippage. The cup sits inside a large stainless steel container which is attached to the top of a 5 cm vertical rotating shaft. The shaft is driven by a variable speed d.c. motor; shear rates can be continuously varied from 0.05 to 750 sec^{-1}. Rotating and stationary chromel–alumel thermocouples are located in the cup and bub, respectively. The complete viscometer assembly resides within a controlled temperature resistance furnace. Finally, slow cooling rates or isothermal experiments can be carried out by controlling the furnace temperature. Whereas, rapid cooling rates, up to 25° C min^{-1} are obtained by incorporating a water spray jacket around the crucible.

2.2. Materials

The metal alloy used throughout this work was Sn–15% Pb which was prepared by melting high purity tin and lead in a resistance furnace. The melt was then cast into the annulus between the cup and bob where it was allowed to completely solidify. The alloy was later completely remelted in the viscometer–furnace assembly before each experiment.

The viscometer was calibrated with U.S. National Bureau of Standards oils (standard number S-60, S-600 and S-2000, conforming to ASTM oil standard). The data agreed to within less than 4%.

To verify the ability of the viscometer to detect and measure thixotropy, experiments were also carried out on well known non-metallic thixotropic materials. Epoxy (Shell EPON 828) containing 2.95 wt % (1.30% by volume) of SiO_2 flakes (Cab.O. Sil), unprocessed honey (New England blend), and paint (Sherwin–Williams, flat-tone, alkyd base) were used.

2.3. Procedure

Initially, the metal alloy in the annulus was completely melted by heating it to above its liquidus temperature. Two different series of experiments were then carried out. In the first series, the alloy was continuously sheared while it cooled at a predetermined rate to a temperature within the liquid–solid range. When the desired temperature, volume fraction solid, was reached, the rotation of the cup was stopped and the specimen was quenched utilizing the water spray jacket around the crucible.

In the second series of experiments the initial processing steps were identical to the above. Shearing was conducted continuously during cooling from above the liquidus temperature. However, the alloy was gradually cooled to a specified temperature in the liquid–solid region, volume fraction solid, and held isothermally. After the torque attained a constant "steady state" value, hysteresis loops were generated to study the thixotropic characteristics of the system. At the end of these isothermal experiments, rotation was stopped and the specimen quenched.

The first series of experiments were aimed at studying the effect of initial processing variables on the viscosity and structure of the partially solidified alloy. The three independent variables were: cooling rate, ϵ, initial shear rate*, $\dot{\gamma}_0$, and the volume fraction solid, g_s. The range of cooling rates employed was 0.33 to 25° C min^{-1}. The lower rates were achieved by furnace cooling the specimen. The high cooling rates were achieved by direct water cooling of the crucible utilizing the spray jacket. Intermediate cooling rates were obtained by air cooling the crucible. Rotation speeds were varied with the two cup and bob arrangements (3 mm and 9 mm spacings) such that shear rates in the range of 115 to 750 sec^{-1} were achieved. Regardless of prior thermal history, at the desired final volume fraction solid, g_{sf}, rotation was stopped and the specimens were quenched at 25° C min^{-1}.

In the second series of experiments, the initial shear rate, $\dot{\gamma}_0$, was maintained until a "steady state" value of torque was achieved. Different cycles of rotation and rest were then applied while the tem-

* Shear rate in these experiments is rererred to as initial shear rate, even though it was the only shear rate used throughout each experiment.

perature, volume fraction solid, of the system was maintained constant. The following series of tests were carried out.

(1) The pseudoplasticity of the slurries was studied by varying the rate of shear and measuring new "steady state" values of torque, viscosity. A different flow curve was thus generated for each initial condition of shear rate, $\dot{\gamma}_0$, and volume fraction solid, g_s.

(2) Hysteresis loops were generated using the Green and Weltmann [2] techniques described earlier. Fig. 5 shows the procedure employed, rotation speed versus time, to generate a hysteresis loop; five independent variables were controlled (one shear rate and four different times). Maximum shear rate, $\dot{\gamma}_{max}$ in Fig. 5 could be varied as desired; it was usually 115 sec^{-1}. The time variables were: (1) down-time, time it took to bring the shear rate to zero, t_d in Fig. 5 (minimum time attainable was 4 sec from 250 sec^{-1} to zero); (2) rest-time, time duration at which no shear was applied, t_r in Fig. 5; (3) up-time, the time it took to go to the desired $\dot{\gamma}_{max}$ at a constant rate of increase, t_u in Fig. 5; and (4) the time during which $\dot{\gamma}_{max}$ was maintained, t_m in Fig. 5.

The number of loops was varied; as many as 75 loops were performed during one experiment; all loop measurements of shear rate versus torque were recorded on an $X-Y$ recorder.

2.4. Metallography

The hollow cylindrical specimen obtained in each experiment was removed from the viscometer, sectioned, polished, etched and metallographically examined. Standard quantitative metallographic techniques were used to determine the size, shape, distribution of size, and volume fraction of primary solid particles (solid particles in the slurry prior to the final quench).

3. Results

3.1. Viscosity and structure of continuously cooled specimens

In these experiments the alloy was continuously sheared and cooled at constant rates from above the liquidus to a given temperature within the liquid–solid region. Volume fraction solid corresponding to a given measured temperature was calculated from the Scheil equation, Appendix 2.

3.1.1. Viscosity

Torque and temperature were continuously monitored during the cooling cycle. Thus, the effects of initial shear rate, $\dot{\gamma}_0$, cooling rate, ϵ, and volume

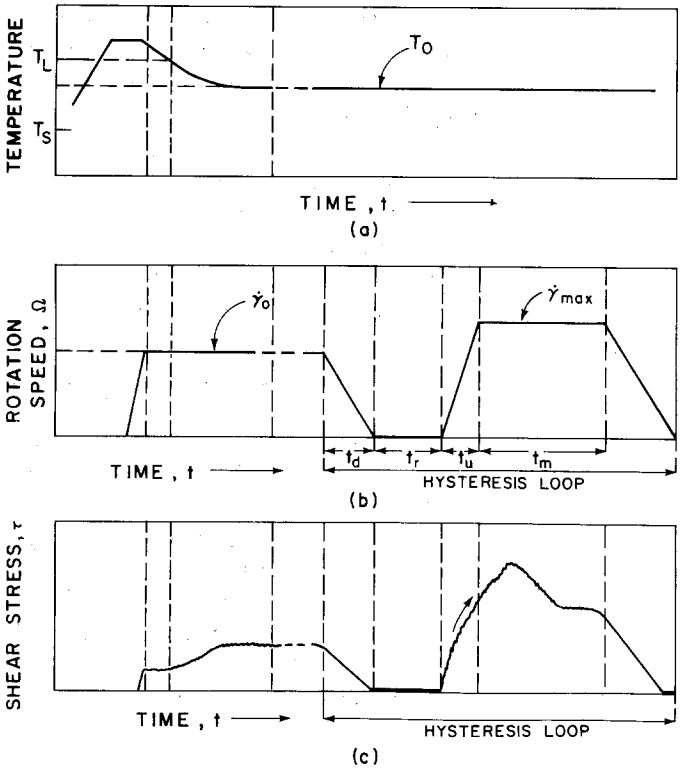

Figure 5 Procedure employed for isothermally held Sn–15% Pb samples showing (a) temperature versus time, (b) rotation speed cycles for a hysteresis loop, and (c) corresponding torque.

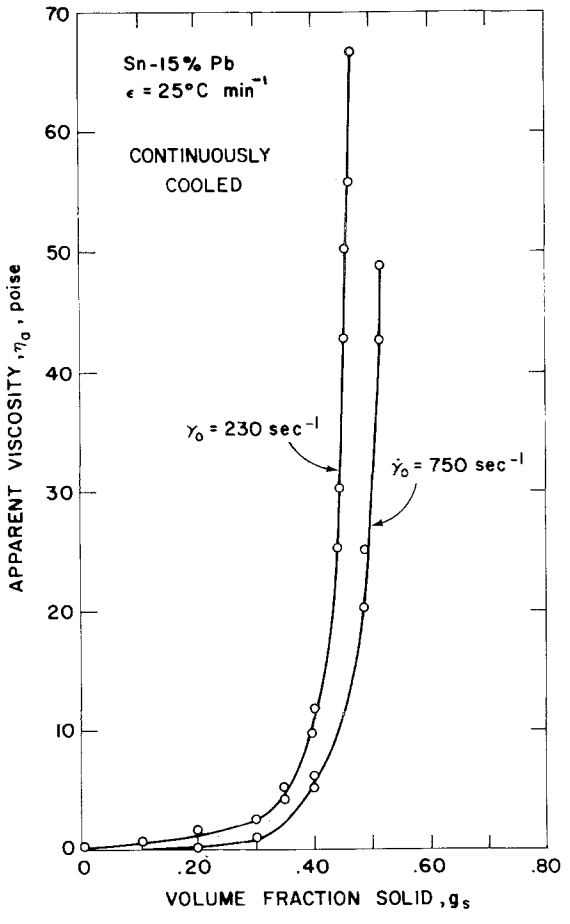

Figure 6 Apparent viscosity versus volume fraction solid of two samples sheared continuously and cooled at a constant rate of 25° C min^{-1}. Initial shear rates 230 and 750 sec^{-1}.

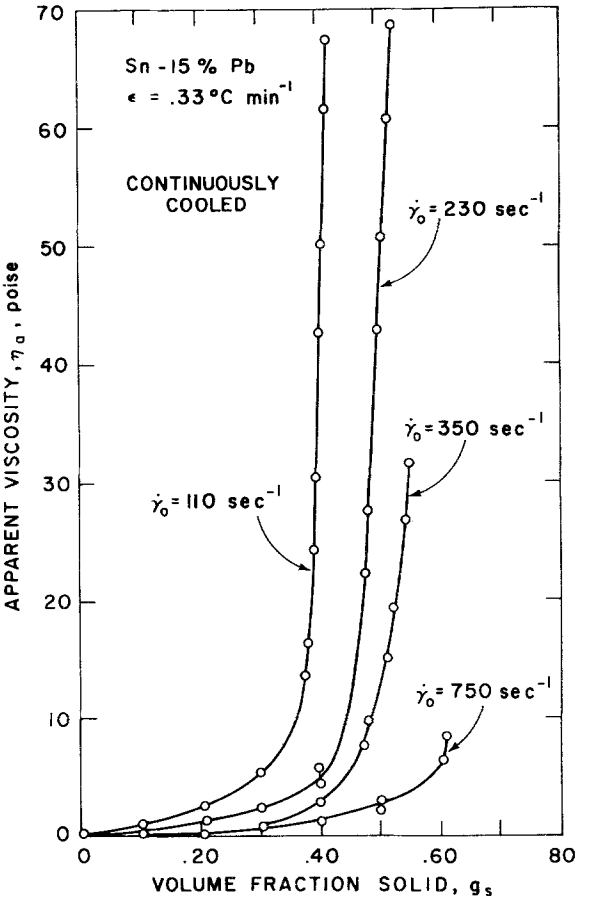

Figure 7 Apparent viscosity versus volume fraction solid of four Sn–15% Pb alloy samples sheared continuously and cooled from above the liquidus temperature at a constant cooling rate of $\epsilon = 0.33°$ C min^{-1}; shear rates, $\dot{\gamma}$, were 115, 230, 350 and 750 sec^{-1}.

fraction solid, g_s, on the apparent viscosity were determined (Figs. 6 to 8).

The following general observations were made. At the liquidus temperature, the apparent viscosity is low; as the temperature drops and liquid freezes, the viscosity begins to rise. The rate of increase is low at first but increases rapidly as the volume fraction solid increases.

Figs. 6 and 7 show that, at a given cooling rate, ϵ, the viscosity decreases with increasing initial shear rate. Fig. 8 shows that, at a given initial shear rate, $\dot{\gamma}_0$, the viscosity decreases as the cooling rate decreases (i.e. as the total time spent in the liquid–solid region increases).

At a high cooling rate, $\epsilon = 25°$ C min^{-1}, an increase in the initial shear rate from $\dot{\gamma}_0 = 230$ to $\dot{\gamma}_0 = 750\,sec^{-1}$ results in a moderate decrease in the viscosity of the slurry (Fig. 6). For example, at $g_s = 0.45$, the viscosity decreases from $\eta_a = 37$ to $\eta_a = 12$ P (by a factor of 3).

At the higher initial shear rate, $\dot{\gamma}_0 = 750\,sec^{-1}$, the viscosity of the slurry can be further reduced by decreasing the cooling rate (Figs. 7 and 8). For example, at $g_s = 0.45$, as the cooling rate is decreased from $\epsilon = 25$ to $\epsilon = 0.33°$ C min^{-1}, the viscosity is reduced from $\eta_a = 12$ to $\eta_a = 2$ P (by a factor of 6).

Some of the data generated in these experiments are listed in Table I. To show the relative change in measured viscosity as a function of cooling rate, initial shear rate and volume fraction solid a composite plot of some of the data from Figs. 6 to 8 and Table I is presented in Fig. 9.

In general then, viscosity increases with increasing volume fraction solid, increasing cooling rate and decreasing initial shear rate. Furthermore, the

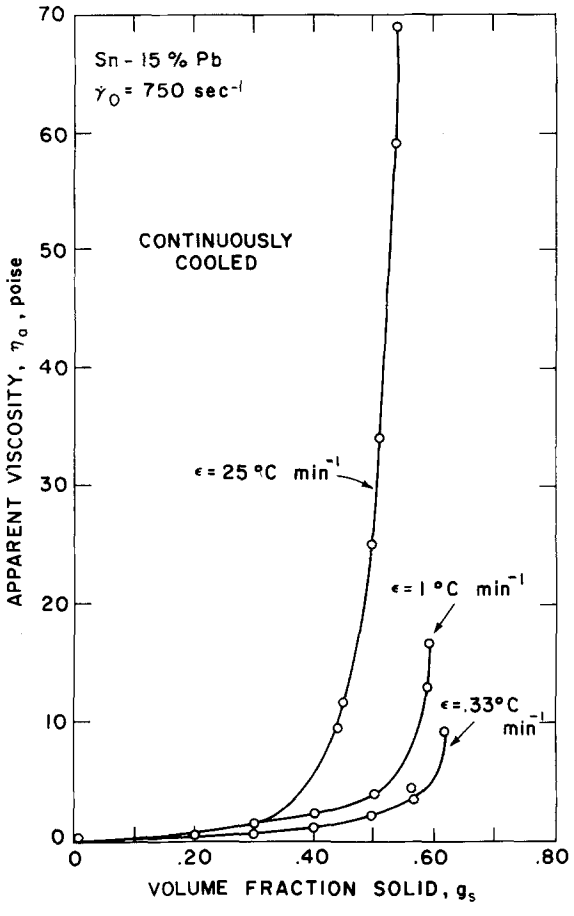

Figure 8 Apparent viscosity versus volume fraction solid of three samples sheared continuously at 750 sec^{-1} and cooled at constant rates of 0.33, 1.0 and 25° C min^{-1}.

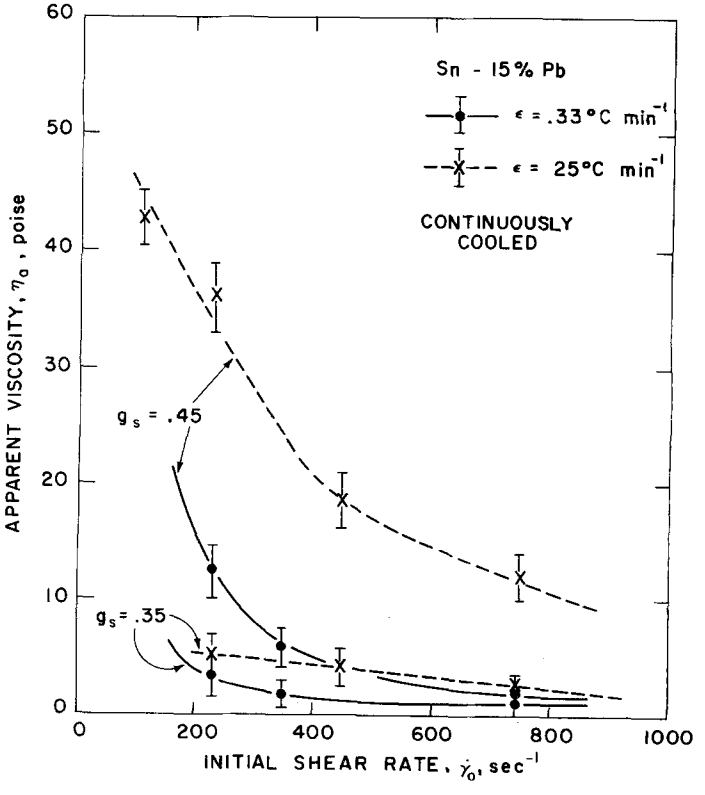

Figure 9 Apparent viscosity versus initial shear rate of samples sheared continuously and cooled at constant rates of 0.33 and 25° C min^{-1}. Curves correspond to volume fractions solid 0.35 and 0.45.

TABLE I Effect of cooling rate, initial shear rate and volume fraction solid on the apparent viscosity of continuously cooled Sn–15% Pb slurries

Volume fraction solid, g_s	Apparent viscosity, η_a (P)							
	Initial shear rate, $\dot{\gamma}_0$ (sec^{-1}) (cooling rate, $\epsilon = 0.33°$ C min^{-1})				Initial shear rate, $\dot{\gamma}_0$ (sec^{-1}) (cooling rate, $\epsilon = 25°$ C min^{-1})			
	115	230	350	750	115	230	450	750
0.20	2.5	1.2	0.4	0.3	1.2	1.2	0.2	0.1
0.30	5.0	2.5	1.0	0.7	2.5	2.5	1.2	1.0
0.35	8.7	3.5	1.7	1.2	4.5	4.5	4.0	2.5
0.40	40.0	5.0	3.0	1.3	13	10	8	6.0
0.45	100	15	6.2	2.0	40	37	18	12
0.50	–	40 ± 10	12.5	2.6	85 ± 10	100 ± 10	42	30
0.55	–	80 ± 15	32	3.0	–	–	–	80

relative change in measured viscosity due to variation of cooling rate and shear rate increases drastically with increasing volume fraction solid.

3.1.2. Structure

Once a predetermined temperature in the liquid–solid region was reached, the rotation of the cup was stopped and the slurry was water quenched as described earlier. The notation g_{sf}, final volume fraction solid, has been adopted to correspond to this temperature. Since the remaining liquid in the slurry was rapidly solidified without experiencing shear, it exhibits a fine dendritic structure and delineates the spheroidal (non-dendritic) primary solid particles*.

3.1.2.1. Effect of cooling rate and shear rate. The size of the primary solid particles in the slurry decreases with increasing cooling rate (Fig. 10). At the highest cooling rate used, $\epsilon = 25°$ C min^{-1}, the average size of primary solid particles (average minor axis, $\bar{X}$) is about 50 ± 20 μm for a final volume fraction solid $g_{sf} = 0.55$, and does not appear to be affected by the shear rate employed (Fig. 10).

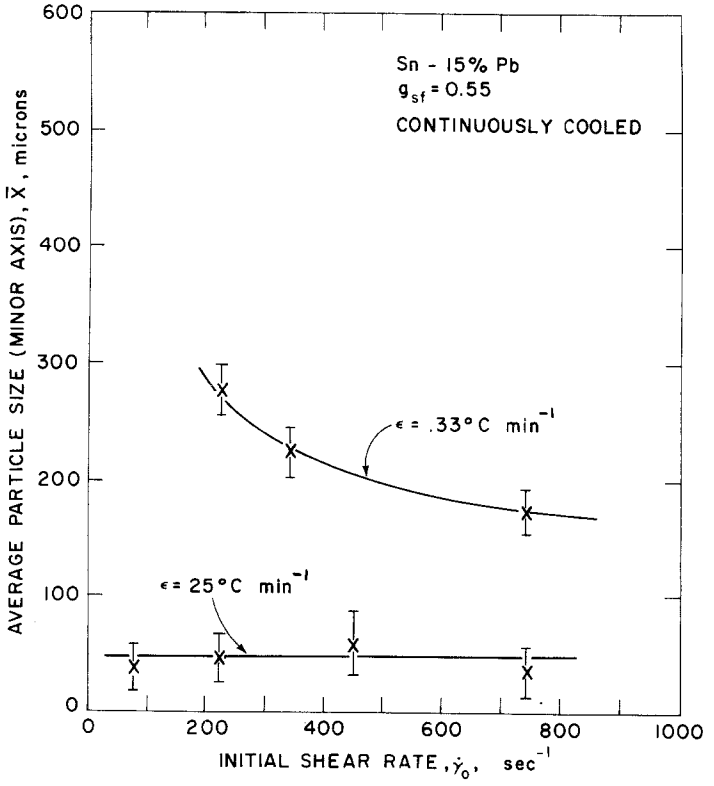

Figure 10 Average size of primary solid particles versus initial shear rate in samples sheared continuously and cooled at constant rates of 0.33 and 25° C min^{-1} to a final volume fraction solid $g_{sf} = 0.55$.

* Primary solid particles are the particles solidified during shear in the liquid–solid range prior to quench.

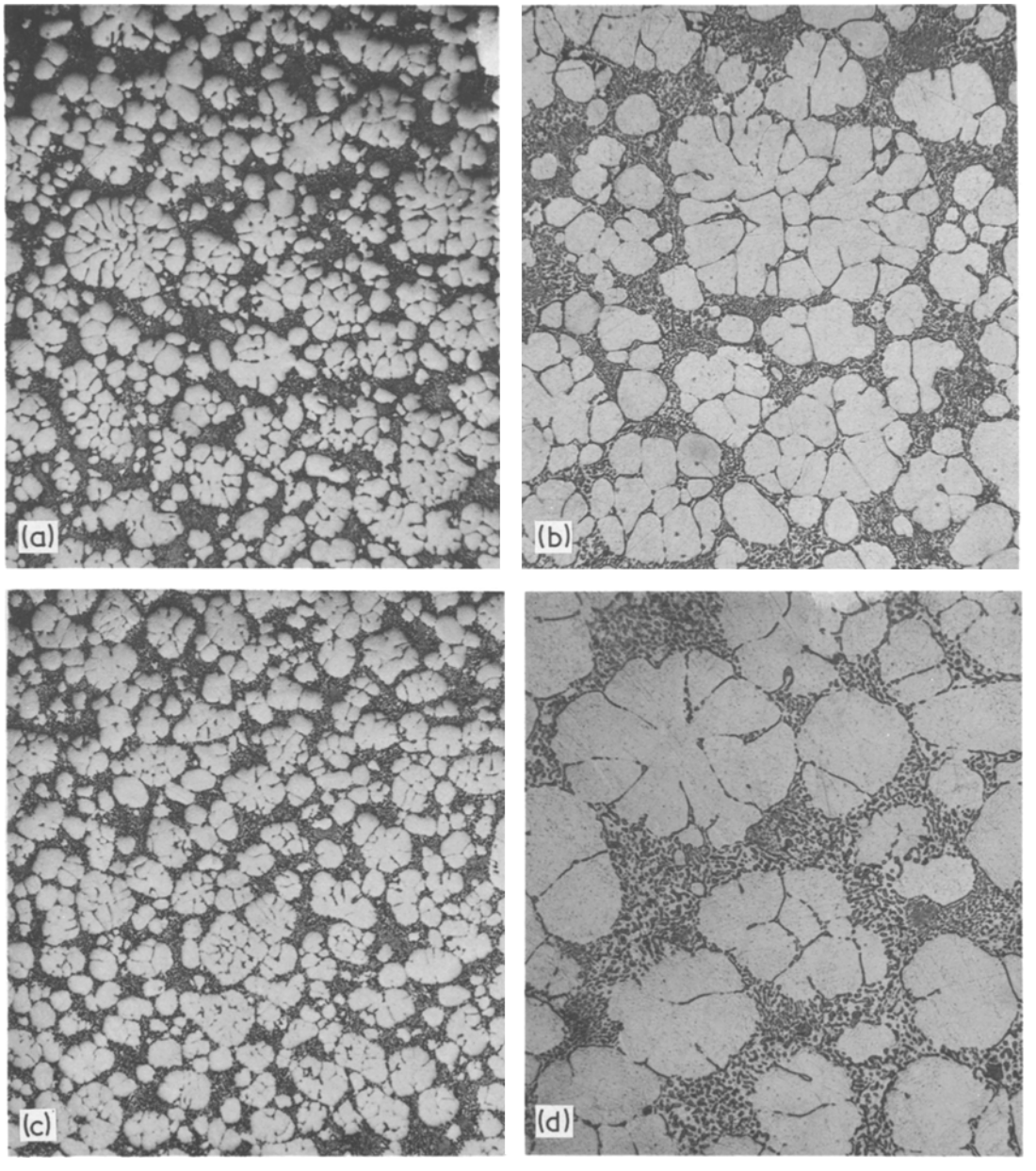

Figure 11 Structure of samples sheared continuously and cooled at a constant rate of 25° C min^{-1} to a final volume fraction solid $g_{sf} = 0.55$; (a) and (b) initial shear rate 230 sec^{-1}, magnification × 45 and × 90, respectively; (c) and (d) initial shear rate 750 sec^{-1}, × 45 and × 90, respectively.

The corresponding microstructures are shown in Fig. 11. The primary solid particles are of the same average size; however, there is less entrapped liquid within the particles that have experienced the higher shear rate, $\dot{\gamma}_0 = 750\,sec^{-1}$. Measured volume fractions of entrapped liquid, from high magnification photomicrographs such as Fig. 11b and d, are 0.13 and 0.08 at $\dot{\gamma}_0 = 230$ and 750 sec^{-1}, respectively.

At the lower cooling rate, $\epsilon = 0.33°\,C\,min^{-1}$, the average size (minor axis) of primary solid particles depends on the shear rate. Fig. 10 shows how the measured size decreases from 275 μm at $\dot{\gamma}_0 =$ 230 sec^{-1} to 175 μm at $\dot{\gamma}_0 = 750\,sec^{-1}$ for a final volume fraction solid $g_{sf} = 0.55$. The corresponding microstructures are shown in Fig. 12. The shape of the primary solid particles remains the same for the range of shear rates used. The amount of entrapped liquid, at this slow cooling rate, is less than

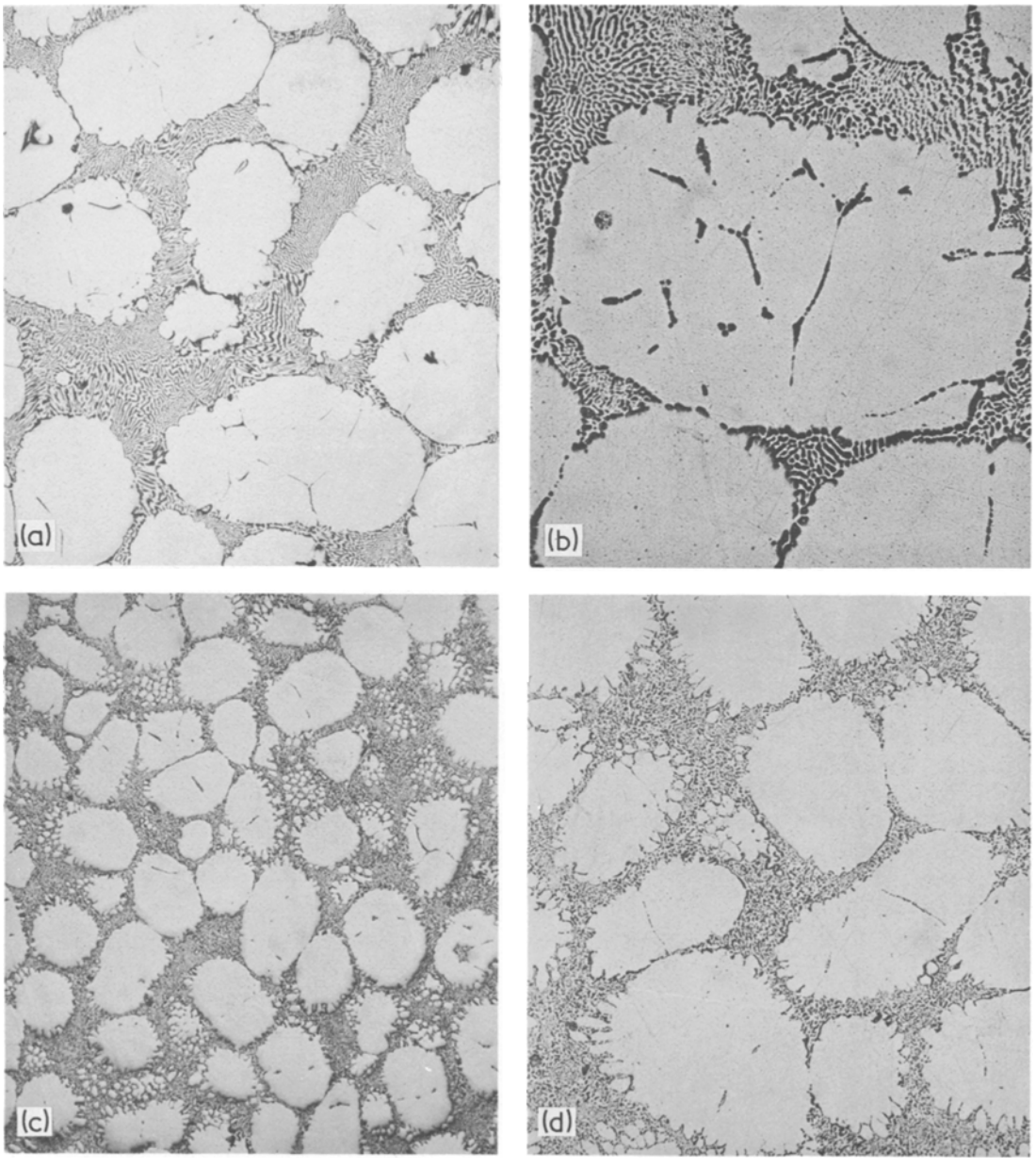

Figure 12 Structure of samples sheared continuously and cooled at a constant rate of 0.33° C min^{-1} to a final volume fraction solid $g_{sf} = 0.55$; (a) and (b) initial shear rate 230 sec^{-1}, × 45 and × 90, respectively; (c) and (d) initial shear rate 750 sec^{-1}, × 45 and × 90, respectively.

that at the higher cooling rate. For example, at $g_{sf} = 0.55$ and $\dot{\gamma}_0 = 230\,sec^{-1}$, the amounts of entrapped liquid are 0.13 and 0.02 for cooling rates of 25 and 0.33° C min^{-1}, respectively. With increasing shear rate, the amount of entrapped liquid in the slow cooled samples becomes negligible (see Fig. 12).

Typical measured distribution of size of primary solid particles for the various processing conditions above are shown in Fig. 13. At the higher cooling rate, $\epsilon = 25°\,C\,min^{-1}$, this distribution is rather broad and does not change much over the range of shear rates used (Fig. 13). The standard deviation, σ_x, was calculated for each specimen – the ratio, $\sigma_x/\bar{X}$, where $\bar{X}$ is the average size (minor axis) of primary solid particles, varies between 0.70 and 0.90. The size distribution of primary solid particles decreases with decreasing cooling rate and in-

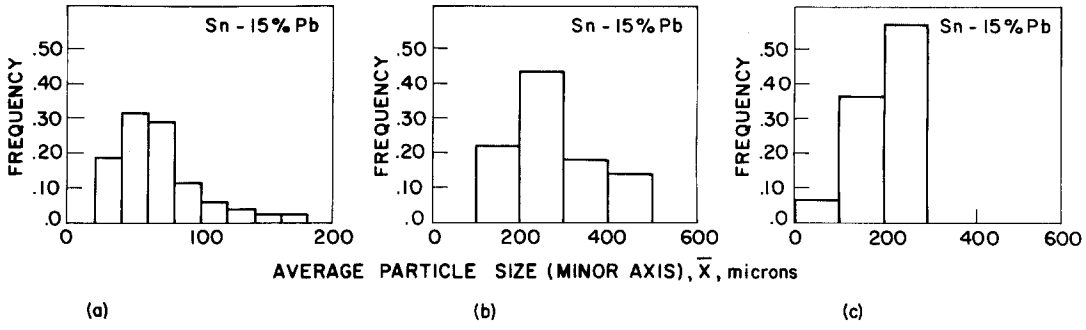

Figure 13 Distribution of size of primary solid particles (average minor axes) in samples sheared continuously and cooled at constant rates to a final volume fraction solid $g_{sf} = 0.55$. (a) $\epsilon = 25^\circ$ C min^{-1}, $\dot{\gamma}_0 = 230$ to 750 sec^{-1}; (b) $\epsilon = 33^\circ$ C min^{-1}, $\dot{\gamma}_0 = 230$ sec^{-1}; (c) $\epsilon = 33^\circ$ C min^{-1}, $\dot{\gamma}_0 = 750$ sec^{-1}.

creasing shear rate (Figs. 13b and c). At the cooling rate of $\epsilon = 0.33^\circ$ C min^{-1}, the values of $\sigma_x/\bar{X}$ are 0.47 and 0.21 for corresponding shear rates of $\dot{\gamma}_0 = 230$ and 750 sec^{-1}, respectively.

In summary then, at the lower cooling rate the primary solid particles in the slurry of Sn–15% Pb alloy are larger, smoother, more uniform in size, and have less entrapped liquid. The amount of this entrapped liquid, hence the effective volume fraction solid in the slurry, decreases with increasing shear rate.

3.1.2.2. Effect of final volume fraction solid. As the final volume fraction of solid in the slurry decreases, it becomes more difficult to distinguish the primary solid particles from the quenched liquid matrix. Most of the dendritic structure grows on existing particles and cooling rate must be abruptly increased to refine this structure, hence delineate the primary solid particles. In specimens that were initially cooled at 0.33° C min^{-1} and quenched at final volume fractions solid $g_{sf} \sim 0.30$, the primary solid particles were distinguishable from the surrounding matrix (Fig. 14a). This was not true for specimens that had experienced the higher initial cooling rate of 25° C min^{-1} (Fig. 14b). It appears that the amount of entrapped liquid within the particles decreases as final volume fraction solid increases (c.f. Figs. 14a and 12c).

3.2. Isothermal studies

In these experiments, the alloy was continuously sheared as in the previous section, however, the cooling rate was gradually brought to zero to achieve a constant temperature in the liquid–solid region. Next, three different types of isothermal (constant volume fraction solid) experiments were performed: (1) "steady state"* experiments – in

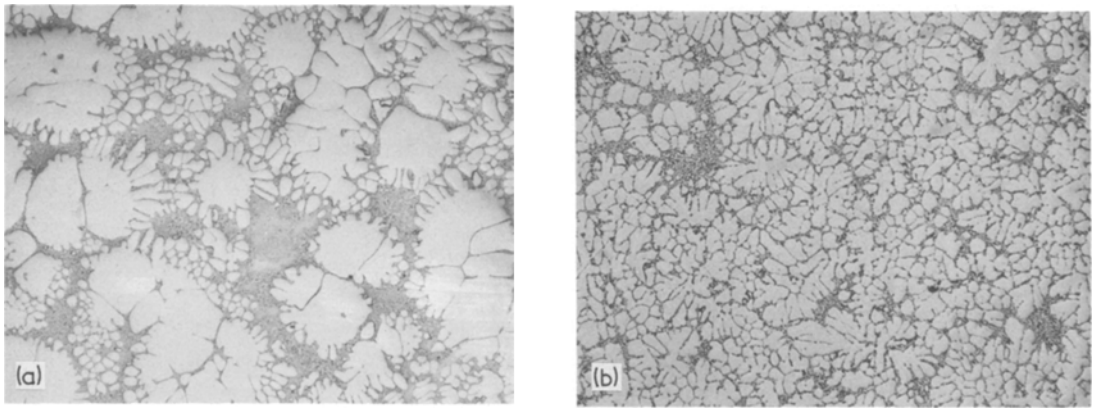

Figure 14 Structure of samples sheared continuously and cooled at constant rates to a final volume fraction solid $g_{sf} = 0.30$; (a) cooling rate 0.33° C min^{-1}, initial shear rate 750 sec^{-1}; (b) cooling rate 25° C min^{-1} initial shear rate 230 sec^{-1} × 40.

* "Steady state" value of torque, or apparent viscosity, is the value obtained when a slurry, regardless of previous thermomechanical history, was held at a given temperature, volume fraction solid, and shear rate until no further observable change in measured torque occurred with time.

which rotation, initial shear rate, was maintained constant and the corresponding "steady state" value of torque was recorded; (2) pseudoplasticity experiments – in which the rotation speed was changed up or down and the new "steady state" value of torque was measured; and (3) thixotropic experiments – in which hysteresis loops were generated using the Green and Weltman [2] techniques.

3.2.1. Viscosity

3.2.1.1. "Steady state". Fig. 15 shows that at a low initial shear rate, $\dot{\gamma}_0 = 115\,\text{sec}^{-1}$, the viscosity of a slurry at a given volume fraction solid above $g_s \sim 0.35$ changes to a lower "steady state" value when the slurry is held isothermally. Fig. 16 shows

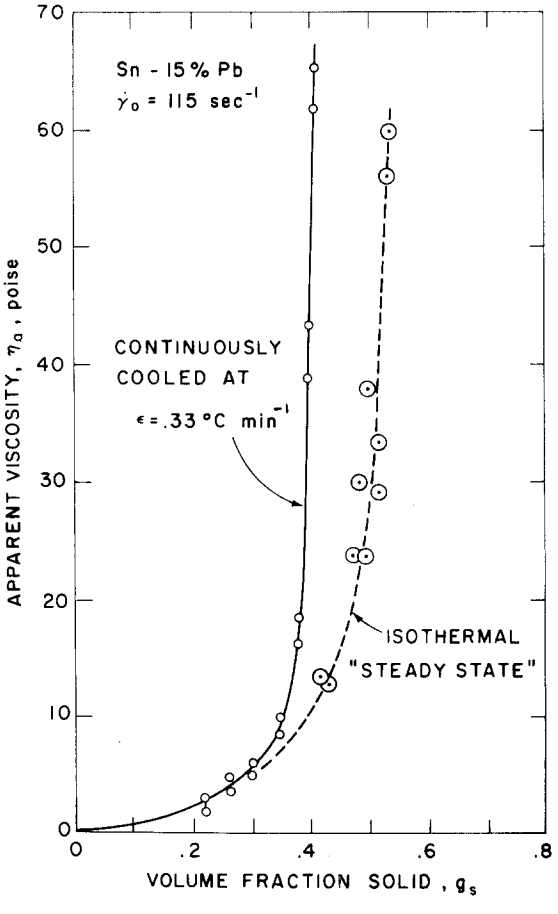

Figure 15 Comparison of the "steady state" apparent viscosities of samples sheared continuously and gradually cooled to a specified temperature, volume fraction solid, and isothermally held with a continuously cooled sample.

that the "steady state" viscosity of an isothermally held slurry, $g_s = 0.45$, decreases with increasing initial shear rate. Each data point on a "steady state" curve is from a separate experiment.

Results of these experiments permit two general observations. First, no change in the viscosity of a slurry was recorded with increasing isothermal holding time after the slurry had spent a total time* of about 60 min in the liquid–solid region. Second, the difference in the viscosity of a continuously cooled slurry and an isothermally held slurry ("steady state" viscosity) decreases with increasing shear rate. This latter point emerges from a comparison of Figs. 7 and 16. For example, at 0.45 volume fraction solid, the viscosity of a slurry continuously cooled at $0.33°\,\text{C}\,\text{min}^{-1}$ and sheared at $230\,\text{sec}^{-1}$ is 15 P compared to 9 P when the slurry is isothermally held; the total times spent in the liquid–solid range were 40 and 90 min, respectively. The corresponding viscosities at shear rates of 350 and $750\,\text{sec}^{-1}$ are 6 and 4 P, and 2 and 1.0 P, respectively.

3.2.1.2. Pseudoplasticity. The procedure here was identical to that reported in the preceding section, except shear rates were changed up or down during isothermal holding and new "steady state" values of torque, apparent viscosity, were recorded. Fig. 17 shows that the "steady state" viscosity of Sn–15% Pb slurry, at a given volume fraction solid, increases with decreasing shear rate. For example, the "steady state" apparent viscosity of a slurry, initially sheared at $115\,\text{sec}^{-1}$ and isothermally held at $g_s = 0.50$, increases from 16 to 75 P as the shear rate is changed over the range of 250 to $30\,\text{sec}^{-1}$. Each curve in Fig. 17 is characterized by the initial shear rate and the volume fraction solid of the slurry. For example, at $g_s = 0.45$, viscosities of a slurry initially sheared at $350\,\text{sec}^{-1}$ are consistently lower than those of a slurry at the same fraction solid but initially sheared at $115\,\text{sec}^{-1}$. These observations are in line with those previously reported in Fig. 16.

Finally, changes in apparent viscosity with shear rate, up and down a given curve in Fig. 17, are reversible and time dependent. For instance, for the slurry (initially sheared at $350\,\text{sec}^{-1}$ and isothermally held at $g_s = 0.45$) the time to reach a

* In these experiments the total time spent in the liquid–solid range signifies time spent during cooling to reach a certain volume fraction solid plus isothermal holding time. In the previous continuously cooled experiments, the total time spent in the liquid–solid range signified time spent during cooling to reach the desired final fraction solid at which rotation was stopped and the specimen quenched.

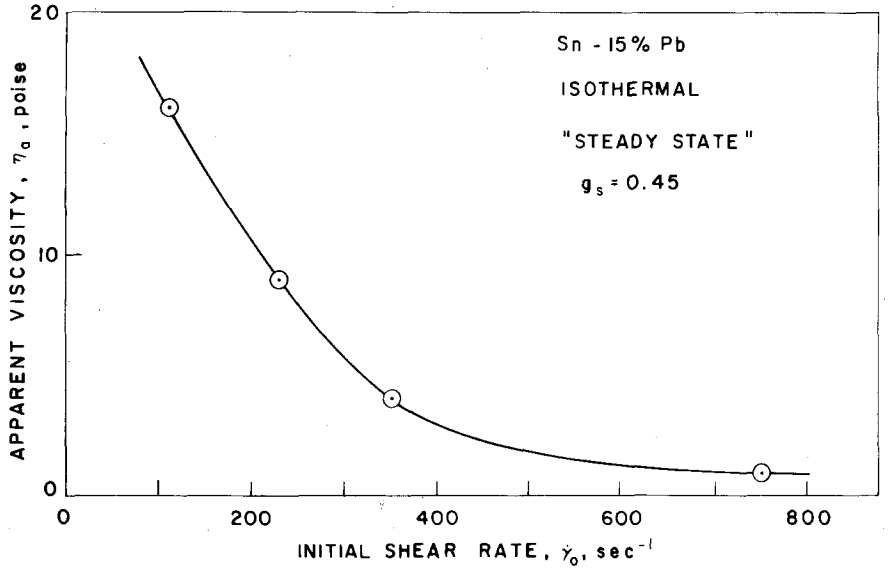

Figure 16 "Steady state" apparent viscosity versus initial shear rate of samples sheared continuously and gradually cooled to 0.45 volume fraction solid and isothermally held. Each sample spent a total time of ~90 min in the liquid–solid region.

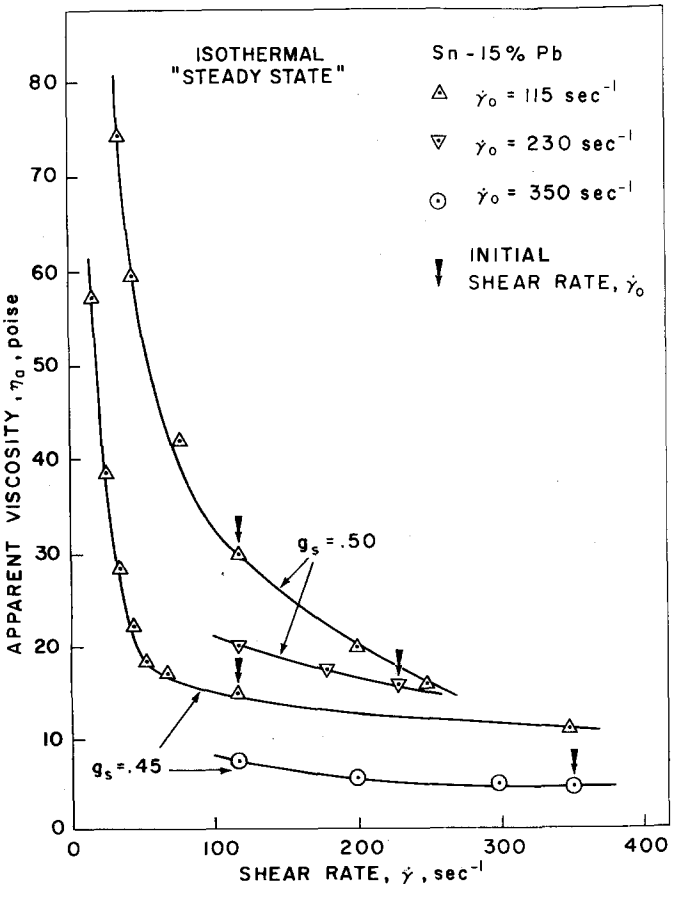

Figure 17 Pseudoplastic behaviour of Sn–15% Pb slurries. Effect of change of shear rate on the "steady state" apparent viscosity. Samples were sheared continuously at different initial rates and held isothermally at volume fraction solid of 0.45 and 0.50 while they were subjected to changes in shear rate.

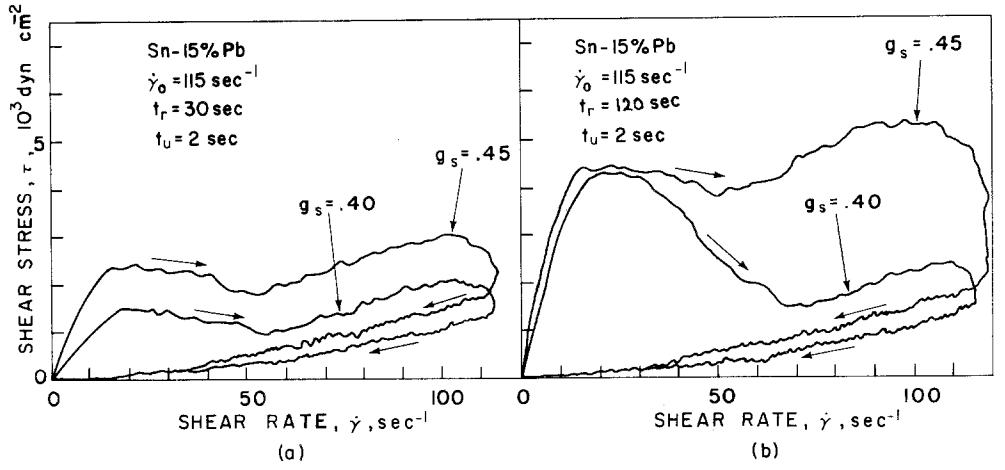

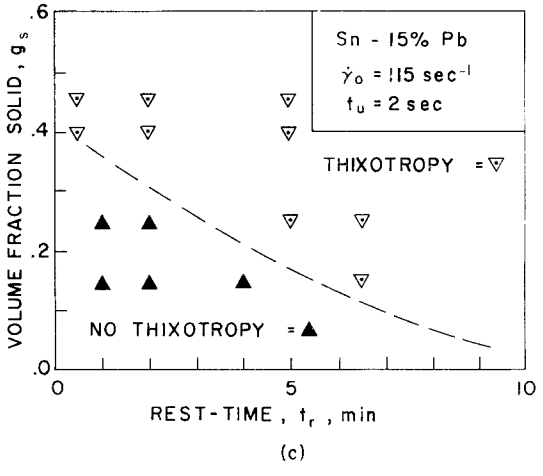

Figure 18 Effect of volume fraction solid on hysteresis loops of isothermally held slurries (a) and (b) loops generated after rest-times of 30 and 120 sec, respectively; (c) observation of measurable thixotropy as a function of volume fraction solid and time at rest.

new "steady state" value of viscosity when shear rate was changed from 150 to 400 sec^{-1} was ~5 min. The thixotropic behaviour of the slurries is characterized below.

3.2.1.3. Thixotropy. The procedure followed in these experiments is shown graphically in Fig. 5. After a "steady state" condition was established in the liquid–solid region, hysteresis loops were generated as described earlier. The effect of the following parameters on the area of the hysteresis loops is presented below: (i) the volume fraction solid at which the loops were generated, g_s; (ii) the previous mechanical history, initial shear rate, $\dot{\gamma}_0$; (iii) the time taken to bring the slurry to rest, down-time, t_d; (iv) the time during which the slurry was left at rest, rest-time, t_r; (v) the time taken to increase the shear rate to its maximum value, up-time, t_u; (vi) the maximum shear rate, $\dot{\gamma}_{max}$.

All the slurries reported here were continuously sheared at an initial shear rate, $\dot{\gamma}_0$, of 115 sec^{-1} * as they gradually cooled to a predetermined isothermal holding temperature. Shear was continued until a total time of ~90 min was spent in liquid–solid region and the "steady state" value of torque measured. Each slurry was then brought to rest during a down-time $t_d = 4$ sec*.

(i) Volume fraction solid. The effect of volume fraction solid on the hysteresis loops is shown in Fig. 18. Up-time to reach a maximum shear rate of $\dot{\gamma}_{max} = 115$ sec^{-1} was 2 sec. The curves in Fig. 18a and b are for two different rest-times of 30 and 120 sec, respectively. For a given rest-time, the area of the hysteresis loop increases with increasing volume fraction solid. For example, at $t_r = 30$ sec, the measured areas for fractions solid $g_s = 0.40$ and $g_s = 0.45$ are 1.15×10^5 and 2.05×10^5 dyn cm^{-2} sec^{-1}, respectively.

For volume fraction solid lower than $g_s \simeq 0.30$, the appearance of thixotropy, i.e. hysteresis loop, depends on the time the slurry is left at rest. Fig. 18c shows the domains where thixotropy and no thixotropy are observed. For example, at $g_s = 0.25$, slurries initially sheared at 115 sec^{-1} did not exhibit thixotropy (i.e. the difference in stress was lower than the accuracy of the stress recorder, $\simeq 10^2$ dyn cm^{-2}) for rest-times of up to about 2 min. Evidence of thixotropy, hysteresis loop, was observed after a rest-time of 5 min. The data presented are for an up-time of 2 sec to reach a maximum shear rate of 115 sec^{-1}.

*Exceptions will be noted.

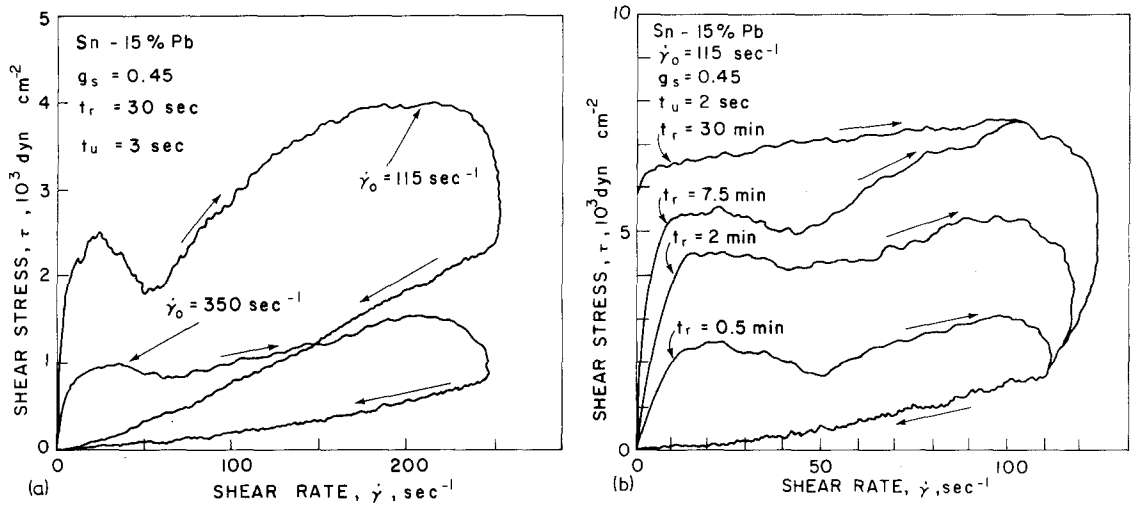

Figure 19 Effects of initial shear rate and rest-time on hysteresis loops of isothermally held slurries (a) effect of initial shear rate, $\dot{\gamma}$, (b) effect of rest-time, t_r.

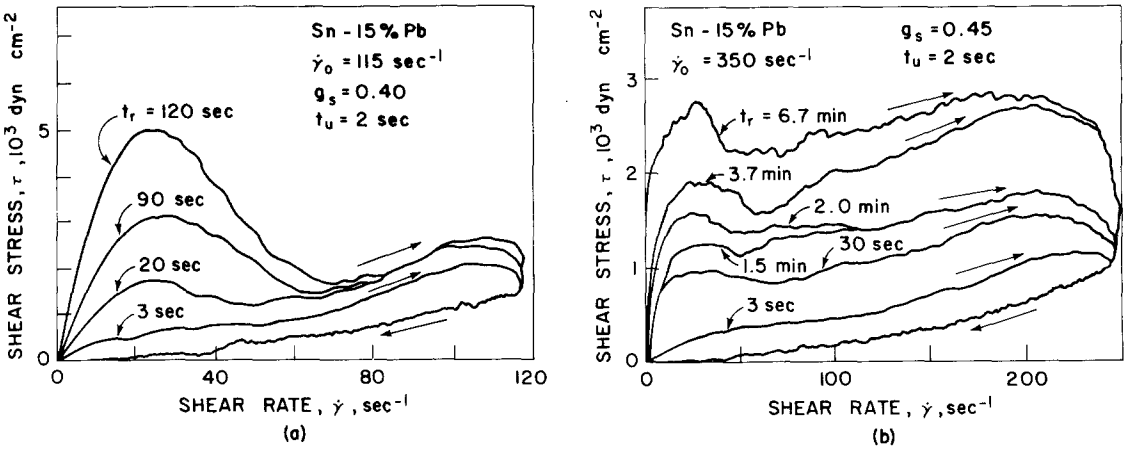

Figure 20 Effects of rest-time, t_r, on hysteresis loops of isothermally held slurries (a) and (b) are for different initial shear rates and volume fractions solid.

(iii) Initial shear rate. The effect of initial shear rate, $\dot{\gamma}_0$, on thixotropy is shown in Fig. 19a. Two slurries, $g_s = 0.45$, were left at rest for 30 sec. Up-time to reach a maximum shear rate, $\dot{\gamma}_{max}$, of 250 sec^{-1} was 3 sec. The area of the hysteresis loops decreases with increasing initial shear rate. It is 6 $\times 10^5$ and 1.55×10^5 dyn cm^{-2} sec^{-1}, for corresponding initial shear rates of 115 and 350 sec^{-1}.

(iii and iv) Down-time and rest-time. The down-time referred to here is time spent in decreasing the shear rate of the slurry from its initial value, $\dot{\gamma}_0$, to zero prior to hysteresis loop measurements. The effects of down-time and rest-time are similar. The area of the hysteresis loops increases with increasing down-time and rest-time. The curves in Figs. 18a and b, and 19b show the effect of rest-time, t_r, on the hysteresis loops obtained with an up-time of 2 sec to reach a maximum shear rate of 115 sec^{-1}. The recorded area of the loops increases with increasing time at rest. The same phenomenon was observed when the fraction solid and the initial shear rate were varied (Fig. 20a and b).

(v) Up-time. The up-time is the time spent in increasing the shear rate from zero to its maximum, $\dot{\gamma}_{max}$. Fig. 21a shows that the area of the hysteresis loops decreases with increasing up-time.

(vi) Maximum shear rate. The effect of maximum shear rate, $\dot{\gamma}_{max}$, on the area of the hysteresis loops is shown in Fig. 21b. The area of the loops increases with increasing maximum shear rate. For

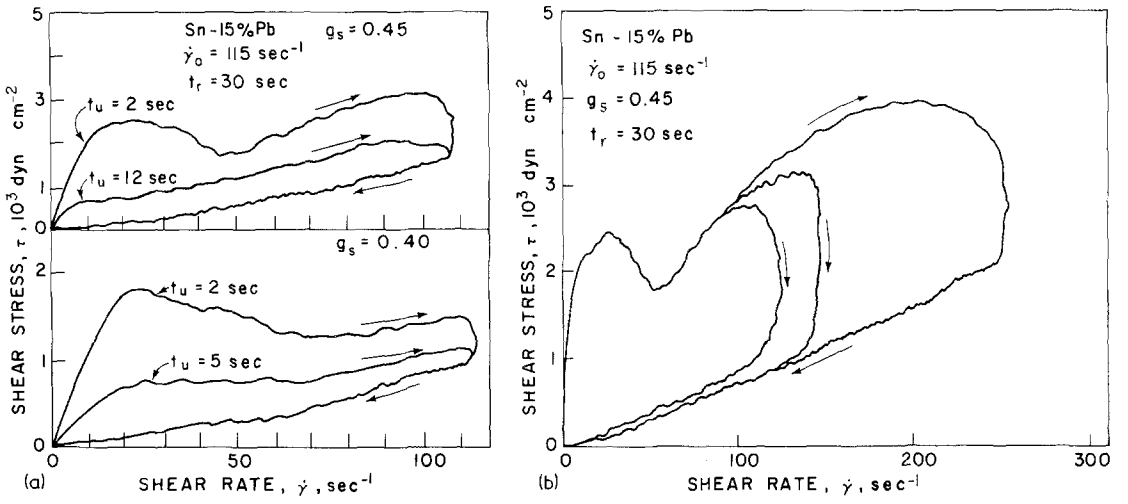

Figure 21 Effects of up-time, t_u, and maximum shear rate, $\dot{\gamma}_{max}$, on hysteresis loops of isothermally held slurries (a) effect of up-time and (b) effect of maximum shear rate.

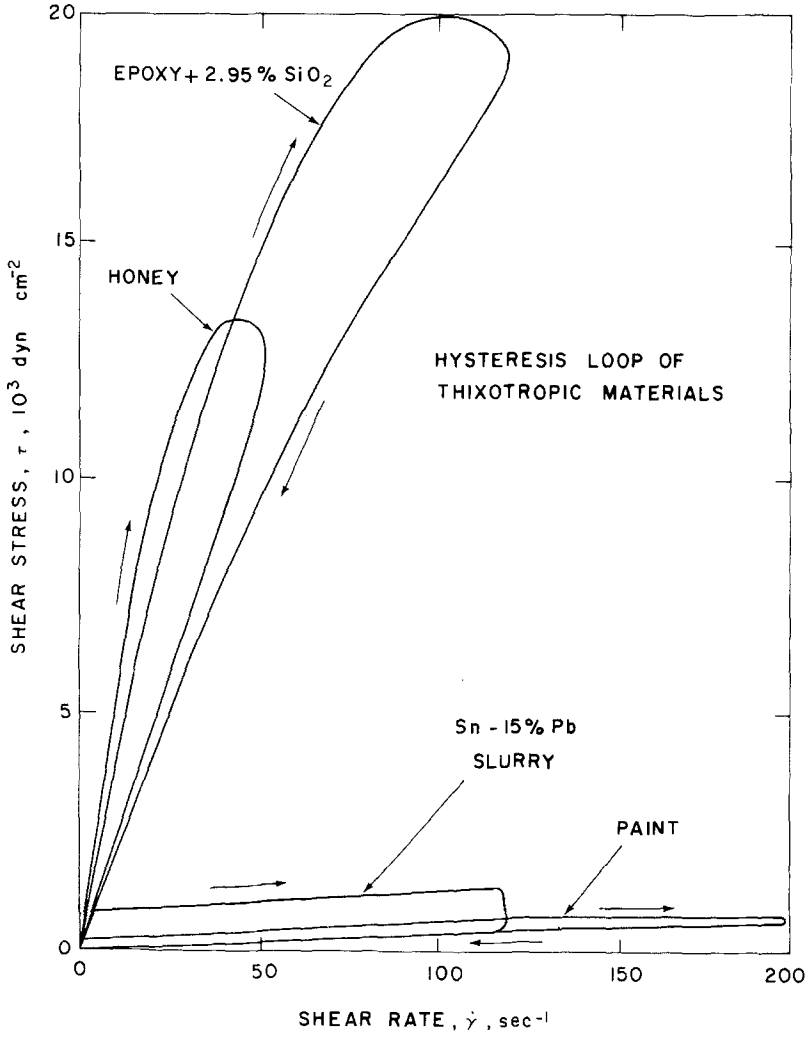

Figure 22 Hysteresis loops of non-metallic systems and a 0.45 volume fraction solid Sn–15% Pb alloy slurry.

instance, the measured area of the loop increases from $\sim 2 \times 10^5$ to $\sim 5 \times 10^5$ dyn cm^{-2} sec^{-1} when maximum shear rate is increased from 115 to 250 sec^{-1}.

Non-metallic systems. Hysteresis loops were also generated for several well known thixotropic systems. Fig. 22 shows a composite plot of these data and a representative hysteresis loop for a 0.45 volume fraction solid slurry of Sn–15% Pb alloy.

In summary, it has been shown that metal slurries are thixotropic for volume fractions solid higher than $g_s \sim 0.30$, regardless of rest-time, and that the area of hysteresis loop is dependent on the thermomechanical history and on the conditions under which the measurements are carried out. For volume fraction solid less than ~0.30, the occurrence of thixotropy, evidenced by a measurable hysteresis loop area in the present apparatus, is a function of the time spent at rest.

The general trends established here are:

(1) the area of the hysteresis loop increases with increasing volume fraction solid, rest-time, down-time and maximum shear rate;

(2) the area of the hysteresis loop decreases with increasing initial shear rate and up-time.

3.2.2. Structure

The important trend established was that the amount of entrapped liquid within the primary solid particles decreases with increasing total time spent in the liquid–solid region. This phenomenon was also observed in the continuously cooled slurries (c.f. Figs. 11 and 12). Fig. 23 shows the structures of three slurries that have been sheared at the same constant initial shear rate of $\dot{\gamma}_0 = 230\,\text{sec}^{-1}$, but have spent different total times in the liquid–solid region. The two slurries in Fig. 23a and b were continuously cooled at 1 and 0.33° C min^{-1} and quenched at a final volume fraction solid $g_{sf} = 0.45$; they spent total times in the liquid–solid region of 13 and 40 min, respectively. The major difference between the structures of these two slurries is the amount of entrapped liquid within the primary solid particles. Fig. 24a shows the decrease in measured volume fraction of entrapped liquid versus total time spent in the liquid–solid region. The effective volume fraction of solid decreases.

Measured average primary solid particle size (minor axis, $\bar{X}$) for the slurries are plotted in Fig. 24a. There is no significant variation in average particles size with total time spent in the liquid–solid

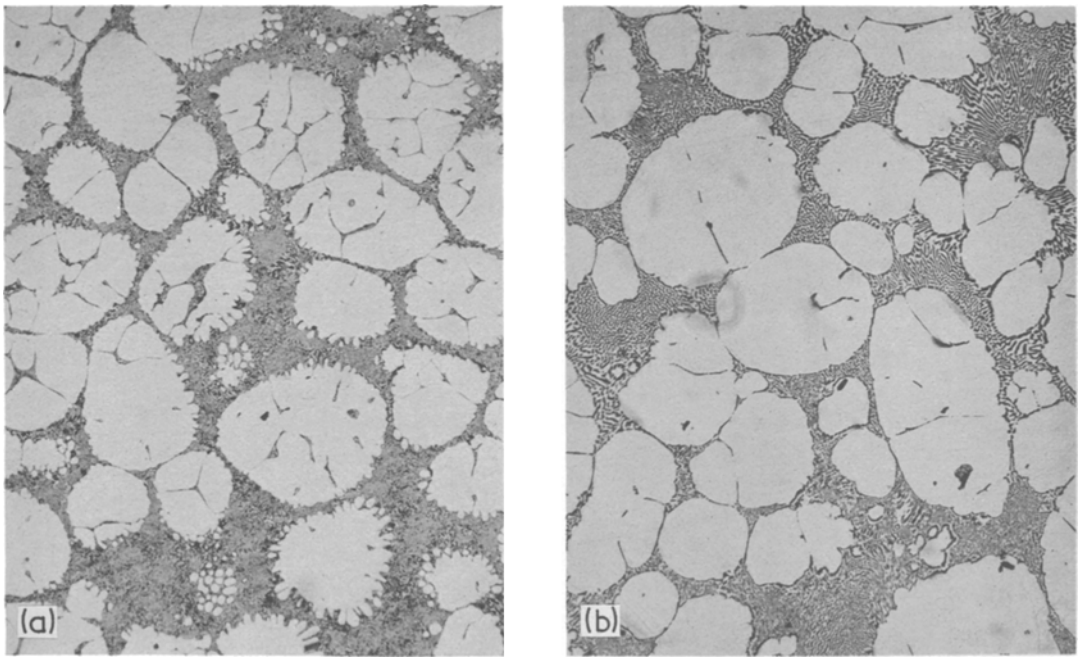

Figure 23 Effect of total time spent in the liquid–solid region on the structure of samples sheared continuously at an initial rate of 230 sec^{-1} and volume fraction solid of 0.45; total time of (a) 13 min (b) 40 min; × 47.

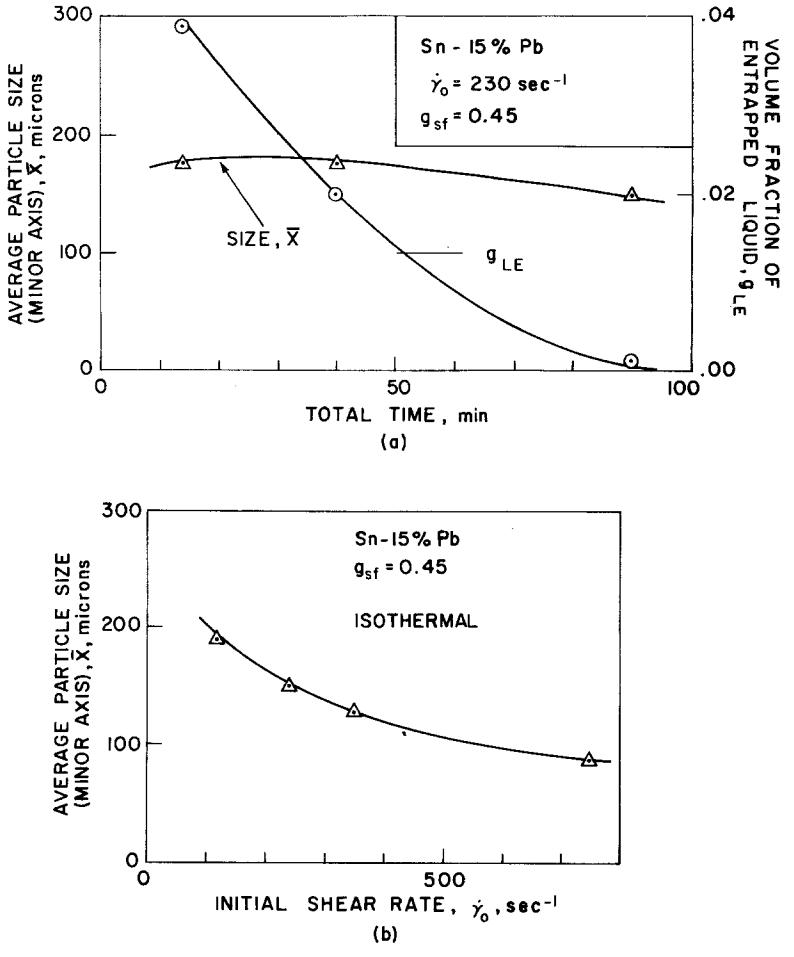

Figure 24 Effect of total time in the liquid–solid region and initial shear rate on average primary solid particle size and amount of entrapped liquid, $g_{sf} = 0.45$; (a) total time, (b) initial shear rate.

region. Of course, as noted earlier (Fig. 10), in continuously cooled slurries (short times spent in the liquid–solid region) particle size decreases with increasing cooling rate.

The effect of initial shear rate on average primary solid particle size was in line with that reported earlier for the continuously (slow) cooled slurries – average particle size decreased with increasing initial shear rate (Fig. 24b).

4. Discussion

Full exploitation of the special rheological properties of vigorously agitated, partially solidified metal slurries in developing new and economical metal-forming processes will require an understanding of the various mechanisms responsible for the formation of the structures. Furthermore, the influence of process variables and physical-chemical properties of the alloy systems of interest on these mechanisms, hence the structure and rheological properties of the slurries should be determined. The work presented here is mainly concerned with the simpler experimentally measurable effects of process variables on the rheological behaviour of the Sn–15% Pb alloy slurries. Attempts to correlate these observations to mechanisms responsible for their occurrences are made only by comparison to previous work on non-metallic systems.

4.1. Effect of volume fraction solid on viscosity

When compared to suspensions of non-interacting spheres of polystyrene, rubber latex, glass and methylmethacrylate [6], the relative viscosity, $\eta_r = \eta_a/\eta_0$, of the metal slurries, at a given volume fraction solid is larger by 1 to 2 orders of magnitude (Fig. 25). The data for the slurries of Sn–15% Pb alloy cover all ranges of thermomechanical treat-

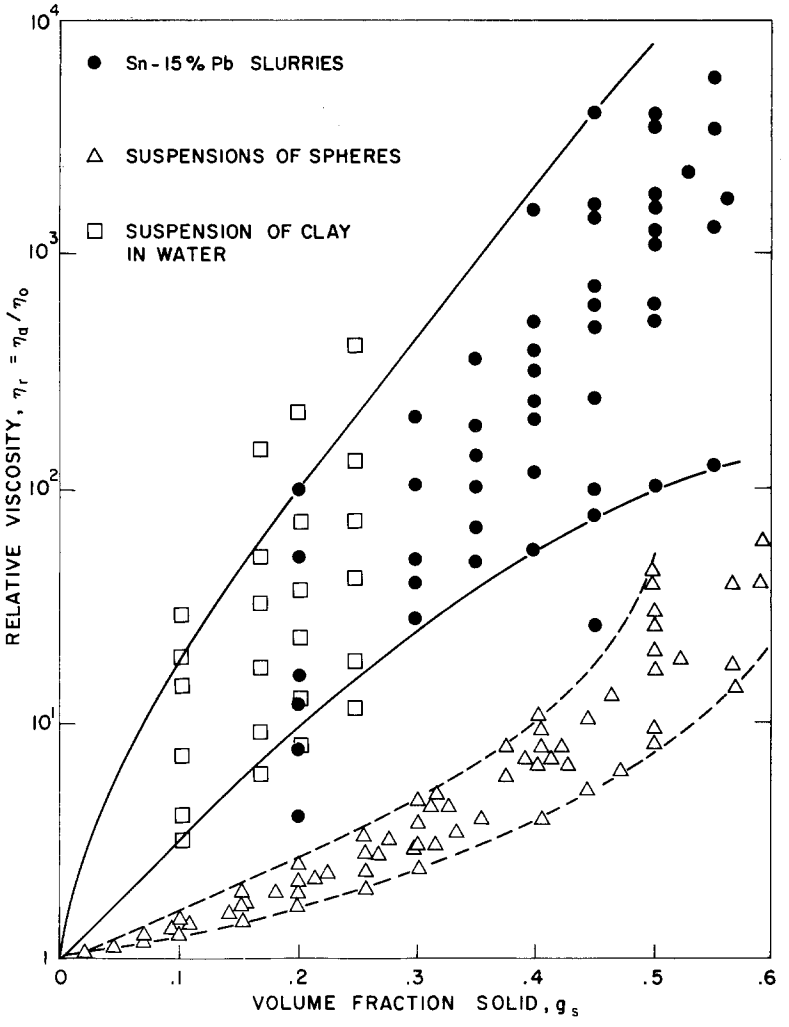

Figure 25 Comparison of the relative viscosity of Sn–15% Pb slurries to that of other suspensions of interacting and non-interacting particles.

ments reported earlier in the results section. The data points for non-interacting spherical particles are for a range of sizes from 0.1 to 435 μm.

When compared to suspensions of Kaolin (clay) particles [7], 0.2 to 2 μm in size, in water, the relative viscosity of the metallic slurries at a given volume fraction solid is of the same order of magnitude (Fig. 25). The data points for Kaolin suspensions cover the range of shear rates from 0.5 to 42 sec^{-1}. The high viscosity of these suspensions has been explained on the basis of an aggregation mechanism [7].

Table II compares relative viscosity data of a partially crystalline polymer [8] (low molecular

TABLE II Comparison of relative viscosity of isothermally held Sn–15% Pb slurries with polyethylene

(a) Isothermally held Sn–15% Pb slurries

Temperature (° C)	Volume fraction solid, g_s	Shear rate, $\dot{\gamma}$ (sec^{-1})			
		115	230	350	750
209.5	0	1	1	1	1
197.6	0.42	540	240	–	–
196.3	0.45	600	400	160	40
195.2	0.47	940	480	–	–
192	0.53	2400	800	–	–
187	0.60	–	2480	–	–

(b) Low molecular weight polyethylene [8]

Temperature (° C)	Shear rate, $\dot{\gamma}$ (sec^{-1})			
	30	100	300	1000
109	1	1	1	1
96	–	–	–	3.98
90	87	1.3	16.6	9.1
84	850	347	151	63
80	3020	930	398	158
70	9350	3540	1520	575

weight polyethylene) to that of the Sn–15% Pb slurries. The relative viscosities of the two systems are of the same order of magnitude. The high viscosity of partially crystalline polyethylene is due to the formation of crystallites. However, in contrast to metallic systems, the degree of crystallinity at a given temperature is a function of shear rate. Therefore, instead of using the degree of crystallinity as a parameter, one may use the degree of molecular association [8] (the molecular weight of the same but amorphous polymer resulting in the same viscosity as that of the partially crystalline polymer). For instance, it is found that the equivalent molecular weight of this polymer increases seven times between its melting point (109° C) and 80° C at a shear rate of 30 sec^{-1} and 3.5 times at a shear rate of 1000 sec^{-1}.

4.2. Effect of structure on viscosity

The general trends established in this study relating viscosity of Sn–15% Pb slurries to their structure (primary solid particle size and volume fraction of entrapped liquid) and thermomechanical processing (i.e. cooling rate and initial shear rate) are summarized in Table III.

In all the continuously cooled and isothermally held slurries, the viscosity at a given volume fraction solid increased with increasing primary solid particle size. The same trend has been reported for suspensions of quartz particles, ranging in size from 25 to 175 μm, in water [3]. In that work, the increase of viscosity was attributed to the increasing magnitude of the inertial forces involved in the collisions of the larger particles.

Table III also shows that a decrease in the amount of entrapped liquid (effective volume fraction solid) results in a corresponding decrease in viscosity. The same effect has been reported for suspensions of aggregates of glass beads, 35 μm in size, in Aroclor (chlorinated biphenyl, $\eta_0 = 80$ P) by Lewis and Nielsen [10]. Each suspension contained only aggregates of a given size (i.e. made up of a fixed number of glass beads) and, therefore, with a constant amount of entrapped liquid. It was shown that by increasing the amount of entrapped liquid (i.e. increasing the size of aggregates) the viscosity of the suspensions increased.

4.3. Equations of state

At high shear rates the apparent viscosity of continuously cooled slurries of Sn–15% Pb alloy plotted versus volume fraction solid on a semi-log paper shows linear dependence over ranges of volume fraction solid (Fig. 26). The linear portions can be described by an equation of the type:

$$\eta_a = A \exp. Bg_s \quad (1)$$

where η_a is the apparent viscosity and g_s is the volume fraction solid. The coefficients A and B are 0.07 and 7.36, respectively, for the cooling rate of 0.33° C min^{-1} and 0.005 and 17.58, respectively, for the cooling rate of 25° C min^{-1}. Equation 1 is identical to the last term of the empirical equation from Thomas' work [6].

$$\eta_r = \eta_a/\eta_o = 1 + 2.5g_s + 10.05g_s^2 + A \exp. Bg_s \quad (2)$$

Thomas proposed that, at volume fractions solid greater than 0.25, the last term in Equation 2 becomes the major contributor to the viscosity of a suspension and is due to the rearrangement of particles under shear. Eyring [11] developed the same kind of relationship assuming that particle rearrangement is proportional to the probability of transfer of particles from one plane of shear to the next.

4.4. Pseudoplasticity

The apparent viscosity of isothermally held slurries of Sn–15% Pb alloy, plotted versus shear rate on a log–log scale shows a linear dependence over cer-

TABLE III Relationship between viscosity and structure of Sn–15% Pb slurries

(a) At a given volume fraction solid

Initial shear rate	Isothermally held specimens			Continuously cooled specimens					
				$\epsilon = 0.33°$ C min^{-1}			$\epsilon = 25°$ C min^{-1}		
$\dot{\gamma}_0$	η_a	$\bar{X}$	g_{Le}	η_a	$\bar{X}$	g_{Le}	η	$\bar{X}$	g_{Le}
↑	↓	↓	↔	↓	↓	↓	↓	↔	↓

(b) At a given volume fraction solid and initial shear rate

Cooling rate $\uparrow\epsilon$, $\uparrow\eta_a$, $\downarrow\bar{X}$, $\uparrow g_{Le}$

g_{Le} = volume fraction of entrapped liquid. ↑, increase; ↓, decrease; ↔ no change.

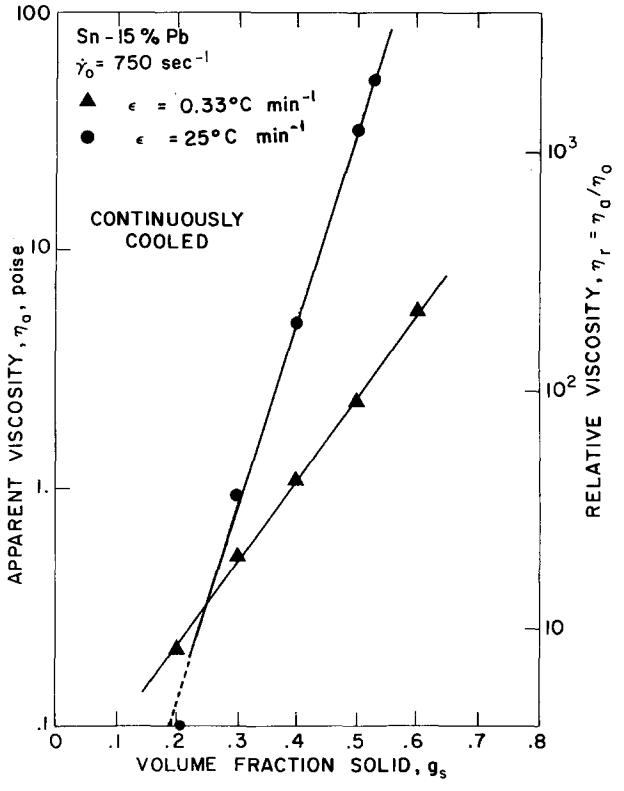

Figure 26 Apparent viscosity versus volume fraction solid of samples sheared continuously and cooled at a constant rate; semi-log plot.

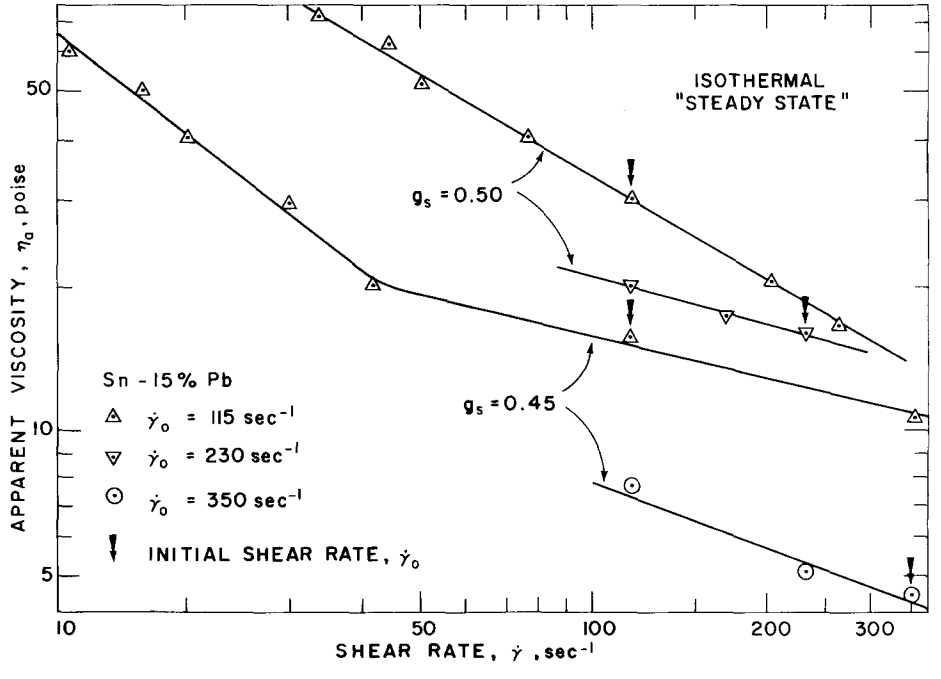

Figure 27 Pseudoplastic behaviour of Sn–15% Pb slurries; effect of charge of shear rate on the "steady state" apparent viscosity; samples were sheared continuously at different initial rates and held isothermally at volume fractions solid of 0.45 and 0.50 while they were subjected to changes in shear rate; log–log plot.

TABLE IV Experimentally determined coefficients of equation 3, $\eta_a = k\dot{\gamma}^n$ relating the apparent viscosity η_a(P) to the shear rate, $\dot{\gamma}$ (sec^{-1})

(a) Isothermally held Sn–15% Pb slurries

	Initial shear rate $\dot{\gamma}_0$ (sec^{-1}) (Volume fraction solid $g_s = 0.45$)			Initial shear rate $\dot{\gamma}_0$ (sec^{-1}) (Volume fraction solid $g_s = 0.50$)	
	115	115	350	115	230
Constant, k Units, egs	380	63	55	830	100
Exponent, n	−0.82	−0.30	−0.44	−0.70	−0.34
Range of shear rates, $\dot{\gamma}$, sec^{-1}	10–40	40–400	100–400	30–300	100–250

(b) Kaolin particles in water [7]

	Volume fraction solid, g_s			
	0.10	0.16	0.20	0.24
Exponent, n	−0.65	−0.74	−0.74	−0.86
Range of shear rates, $\dot{\gamma}$ (sec^{-1})	0.5–10	1–10	1–10	1–10

(c) Partially crystalline polymer [12]

	Temperature (° C)	
	90	80
Exponent, n	−0.50	−0.81
Range of shear rates, $\dot{\gamma}$ (sec^{-1})	100–1000	100–1000

(d) TiO_2 in water [12]

	Volume fraction solid $g_s = 0.40$
Exponent, n	−0.75
Range of shear rates, $\dot{\gamma}$ (sec^{-1})	0–400

tain ranges of shear rates (Fig. 27). The viscosity obeys the following equation:

$$\eta_a = k\dot{\gamma}^n \qquad (3)$$

where η_a is the apparent viscosity, and $\dot{\gamma}$ is the shear rate. The values of the coefficients k and n, calculated from Fig. 27, are listed in Table IV. Equation 3 is the classical power law equation used to describe the flow behaviour of shear rate dependent materials with a negative coefficient, n, for pseudoplastic materials and a positive coefficient, n, for dilatant materials.

The values of n calculated for Sn–15% Pb slurries are of the same order of magnitude as those reported for suspensions of TiO_2 [12] and of Kaolin [7] particles in water (Table IV). Kaolin particles were shown to form aggregates whose size decreases with increasing shear rates. Reducing the size of the aggregates results in lowering of the effective fraction solid (reduced entrapped liquid) and a corresponding decrease in viscosity.

.The partially crystalline polymer (low molecular weight polyethylene) follows Equation 3 over certain ranges of shear rates [8]. The experimentally determined values of the coefficient n are given in Table IV and are of the same order of magnitude as those for Sn–15% Pb slurries. Two mechanisms were proposed to explain this observation [8] : (1) the high shear rates "melt" or destroy the crystallites (it was found that the equivalent molecular weight decreases with increasing shear rate) and (2) high shear rates orient assymetric aggregates in the direction of flow. This latter mechanism was also found to occur for liquid crystals that exhibit the same type of behaviour [13].

Some of the proposed mechanisms outlined above are for aggregates of micron size (flocs) and needle shaped particles (kaolin, TiO_2) and some are for macromolecular aggregates (polyethylene). These mechanisms cannot be directly applied to metal slurries. However, the basic explanation of pseudoplasticity is based on models where there is an equilibrium between the rate of build-up and breakdown of aggregated structure; the build-up is due to the aggregation of particles or molecules to lower their surface energy and the breakdown is caused by the stresses due to the fluid flow forces acting on the aggregates.

4.5. Thixotropy

When compared to other thixotropic systems, metal slurries of Sn–15% Pb alloy exhibit a degree of thixotropy (area of hysteresis loop) of the same

order of magnitude as that of the non-metallic systems used for comparison in this study (Fig. 22). As an example, the measured areas of hysteresis loops for the Sn–15% Pb slurries at a fraction solid of 0.45, honey, and epoxy with 2.95 wt% SiO_2 are 2 to 8, 1.0, and 3.0 x 10^5 dyn cm^{-2} sec^{-1}.

The structure of a thixotropic material is both shear rate and time dependent, as is its measured viscosity. At low shear rates it is made up of aggregates with an effective volume fraction solid larger than the actual volume fraction solid present, due to entrapped liquid. With increasing shear rates, fluid flow forces break down the aggregates into smaller particles with less entrapped liquid, thus reducing the viscosity of the material. The observation of the hysteresis loop is a consequence of the time dependence of the dissaciation of the aggregates.

In the case of chemically non-interacting particles, the aggregation (particle flocculation) at low shear rates is due to the attractive forces between the particles, e.g. long range electrical forces which permit the individual particles of, for example, clay to interact over distances of the order of 1000 Å [7]. This aggregation can also be due to the formation of welds between chemically interacting particles such as the primary solid particles of Sn–15% Pb slurries. To differentiate between interacting and non-interacting particles, aggregation of the former is referred to as agglomeration and the latter as flocculation.

For thixotropy to be observed, the concentration of the solid phase must be large enough to permit a significant number of particles to aggregate. In the case of chemically interacting particles, agglomerates form when two particles collide and stay in contact long enough for a weld to form. The probability of successful collisions (collisions followed by weld formation) depends on size, shape, number and distribution of size of primary solid particles as well as on shear rate.

The general trends established in this study relating the degree of thixotropy (area of hysteresis loop) to the structure and thermomechanical history of isothermally held slurries of Sn–15% Pb alloy are shown in Table V. An important finding of this work is that for a given time at rest, there is a minimum volume fraction solid below which no thixotropy is observed (Fig. 18). For example, below volume fractions solid $g_s \sim 0.30$ for rest-times of up to 2 min the areas of the hysteresis loops of Sn–15% Pb slurries are below the measurable minimum of approximately 0.1 x 10^5 dyn cm^{-2} sec^{-1}. Increasing the rest-time or the volume fraction solid beyond these limits results in corresponding increases in the area of the hysteresis loop, hence increased thixotropy.

TABLE V Relationship between degree of thixotropy (area of hysteresis loop) and the independent variables in isothermally held slurries of Sn–15% Pb alloy

An increase in the variable	Results in a corresponding
g_s	increase in A
$\dot{\gamma}_0$	decrease in A
t_r	increase in A
t_d	increase in A
t_u	decrease in A
$\dot{\gamma}_{max}$	increase in A

A = area of hysteresis loop

5. Conclusions

5.1. General

The apparent viscosity of Sn–15% Pb slurries increases with increasing volume fraction solid and is structure dependent. The structure and apparent viscosity are strongly influenced by the thermomechanical history of the alloy during solidification. The rheological behaviour of vigorously agitated slurries of the alloy exhibit thixotropy.

5.2. Continuously cooled slurries

(1) The viscosity of the slurry, at a given volume fraction solid, decreases with decreasing cooling rate and increasing shear rate. Exercising the full range of shear and cooling rates possible in the viscometer the apparent viscosity of a 0.55 volume fraction solid slurry was varied from 3 to 80 P.

(2) In general, the size of the primary solid particles is in the range of 50 to 300 μm. It increases with increasing volume fraction solid and decreasing cooling rate. Increasing the shear rate always reduces the amount of entrapped liquid in the particles. However, it is effective only in reducing the particle size at slow cooling rates.

(3) Over wide ranges of volume fraction solid, the apparent viscosity of the continuously cooled slurries sheared at 750 sec^{-1} follow a state equation, relating the apparent viscosity, η_a, to the volume fraction solid, g_s.

(4) Comparison of Sn–15% Pb slurries to suspensions of interacting and non-interacting particles, at the same volume fraction solid, shows that the viscosity of metal slurries is of the same

order of magnitude as that of the former and consistently higher than that of the latter.

5.3. Isothermally held slurries

(1) The structures and viscosity of isothermally held slurries follow the same trends as those of slowly cooled slurries. Furthermore, at a given volume fraction solid and shear rate, the viscosity of an isothermally held slurry is lower than that of a continuously cooled slurry.

(2) Variations up or down of shear rate, at a given volume fraction solid, result in a corresponding decrease or increase in the measured viscosity.

(3) Slurries of Sn–15% Pb alloy are thixotropic and show a hysteresis loop phenomenon similar to other well-known non-metallic thixotropic systems. Measured areas of hysteresis loop increase with increasing volume fraction solid, initial viscosity (structure) and time at rest.

(4) The occurrences of thixotropy (defined herein as a measurable minimum hysteresis loop area of 0.1×10^5 dyn cm^{-2} sec^{-1}) is a function of volume fraction solid and time at rest. For volume fractions solid below ~0.30 and rest times of up to 2 min, the areas of the hysteresis loops are below the measurable minimum.

Appendix 1. Dimensions of apparatus and calculations of apparent viscosity

The apparent viscosity of a non-Newtonian fluid is the viscosity a Newtonian fluid would have if it produced the same torque at the same speed. The shear stress on the bob, τ_{bob}, is calculated from the torque, T,

$$\tau_{bob} = \frac{T}{2\pi h \kappa^2 R^2} = CT \qquad (A.1)$$

where h is the height of the bob; R, the radius of the cup, and κ, the ratio of the bob-to-cup radius (see Fig. 4).

The shear rate is defined as

$$\dot{\gamma} = r \frac{d\dot{\theta}}{dr} \qquad (A.2)$$

where $\dot{\theta}$ is the angular velocity at distance r calculated from the equations of motion [14] and is equal, in the case of a Newtonian fluid, to

$$\dot{\gamma}_{bob} = \frac{2\Omega}{1-\kappa^2} \qquad (A.3)$$

where Ω is the angular velocity of the cup.

The apparent viscosity is

$$\eta_a = \frac{1-\kappa^2}{4\pi h \kappa^2 R^2} \frac{T}{\Omega}. \qquad (A.4)$$

The relative error committed by using Equation A3 rather than a more complex equation taking into account the variation of shear rate with position across the annulus, can be evaluated [15] and was equal to 8% maximum for $g_s = 0.45$ and $\dot{\gamma}_0 = 115\,\text{sec}^{-1}$.

The following instrument characterstics were used.

h(cm)	κR(cm)	R(cm)	κ	κ^2	$1/\kappa$	C(cm^{-3})*
8.9	2.225	3.015	0.739	0.545	1.35	3.65
8.9	2.860	3.175	0.900	0.810	1.11	2.40

*Instrument constant.

For the approximate 3 mm gap arrangement, Equation A3 becomes

$$\dot{\gamma}_{bob} = 10.05\,\Omega = 1.05 \text{ rpm} \qquad (A.5)$$

and Equation A4 becomes

$$\eta_a = 0.0002 \frac{T}{\Omega}. \qquad (A.6)$$

Finally, the relative viscosity, η_r, is defined as

$$\eta_r = \frac{\eta_a}{\eta_0}. \qquad (A.7)$$

$\eta_0 = 0.025$ P, is the viscosity of the liquid Sn–Pb alloy at temperatures of interest.

Appendix 2. Calculation of volume fraction solid

Fraction solid can be calculated as a function of temperature from the Scheil equation and the lever rule. The former assumes no solid diffusion, equilibrium at the liquid–solid interface, complete diffusion in the liquid and constant partition coefficient k. The latter assumes complete diffusion in the solid. In the Sn–15% Pb alloy, the difference between these two calculations is negligible. Both equations are deduced from a mass balance and give fraction solid in weight fraction. Difference between calculated weight fraction and volume fraction in this alloy is very small (approximately 0.02) due to small differences in the density of the liquid and the solid.

In this work, the Scheil equation was used without density corrections. The equation is

$$g_s = 1 - \left(\frac{T_M - T_L}{T_M - T}\right)^{1/1-k} \qquad (A.8)$$

where g_s is volume fraction solid; T_M, melting point of pure tin; T_L, liquidus temperature of Sn–15% Pb alloy; and T, actual temperature in the liquid–solid range.

Acknowledgements

This work was sponsored by the Army Research Office, Durham, North Carolina, and was carried out at the Massachusetts Institute of Technology. Frequent and helpful discussions with Professor M.C. Flemings of the Massachusetts Institute of Technology are gratefully acknowledged.

References

1. D. B. SPENCER, R. MEHRABIAN and M. C. FLEMINGS, *Met. Trans.* **3,** (1972) 1925.
2. H. GREEN and R. N. WELTMANN, *Ind. Eng. Chem. An. Ed.* **15** (1943) 201.
3. M. C. FLEMINGS and R. MEHRABIAN, *Trans. AFS* **81** (1973) 81.
4. R. G. RIEK, A. VRACHNOS, K. P. YOUNG, N. MATSUMOTO and R. MEHRABIAN, *Trans. AFS* **83** (1975) 25.
5. R. MEHRABIAN and M. C. FLEMINGS, "New Trends in Materials Processing", American Society for Metals, in press.
6. D. G. THOMAS, *J. Colloid Sci.* **20** (1965) 267.
7. A. S. MICHAELS and J. C. BOLGER, *I.E.C. Fundamentals* **1 (3)** (August, 1962) 153.
8. R. S. PORTER and J. F. JOHNSON, *Trans. Soc. Rheology* **11** (1967) 259.
9. B. CLARKE, *Trans. Instr. Chem. Engrs.* **45** (1967) 251.
10. T. B. LEWIS and L. E. NIELSEN, *Trans. Soc. Rheology* **12** (1968) 121.
11. H. EYRING and D. HENDERSON, "Statistical Mechanics and Dynamics" (Wiley, New York, 1964) p. 460.
12. H. D. JEFFERIES, *J. Oil Colour Chem. Assoc.* **45** (1962) 681.
13. J. HERMANS JUN., *J. Colloid Sci.* **17** (1962) 638.
14. R. BIRD, W. STEWARD and E. LIGHTFOOT, "Transport Phenomena" (Wiley, New York, 1960) p. 94.
15. VAN WAZER *et al.*, "Viscosity and Flow Measurement", (Interscience, New York, 1963) p. 55.

Received 5 January and accepted 27 January 1976.